

1 The Explicit Role of Anion States in High-Valence Metal Oxides

George Sawatzky and Robert Green
Stuart Blusson Quantum Matter Institute and
Max Planck/UBC Centre for Quantum Materials
University of British Columbia
2355 East Mall, Vancouver BC, Canada V6T 1Z4

Contents

1	Introduction	2
2	The importance of anion states	3
2.1	Hole doped states in divalent Cu and Ni oxides	4
2.2	Similar effects in undoped negative charge transfer compounds	5
3	Classification of correlated compounds	8
3.1	Mott-Hubbard and charge-transfer insulators	8
3.2	Mixed valence and negative charge transfer insulators	10
4	Negative charge transfer compounds	12
4.1	Perovskite rare-earth nickelates	12
4.2	Perovskite bismuthates	16
4.3	Other negative or small charge transfer compounds	18
5	Mixed valent rare-earth compounds	20
6	Summary	27

1 Introduction

Correlated metal-oxide compounds exhibit a wide range of interesting properties, including for example high-temperature superconductivity, metal-insulator transitions, and various forms of orbital and magnetic ordering. Many of these metal-oxide compounds with especially interesting properties contain cations which have exceptionally high oxidation states, when one assigns those oxidation states using the usual formal valence-counting methodologies. Transition-metal elements from the $3d$, $4d$, and $5d$ series can usually attain several different oxidation states in compounds, ranging for example from $2+$ to $5+$ for vanadium in oxides. Given this flexibility of the cations, one usually assumes a closed valence shell structure for the anions, meaning that the chalcogens (O, S, Se, Te) would have a $2-$ valence and the halides (F, Cl, Br, I) would have $1-$. Similarly, fixed cation valences according to closed shells are usually assumed for certain columns of the periodic table, including $1+$ for the alkali elements under Li, $2+$ for the alkaline earth elements under Be, and $3+$ for those under Sc and B.

In these standard valence-counting formalisms where anion and the above cation valences are fixed, the remaining cations then adopt the compensating valence to end up with a charge neutral unit cell or formula unit. Following this approach, Fe in FeS_2 would be $4+$, Ni in the rare-earth (R) nickelates $R\text{NiO}_3$ would be $3+$, and there would be Cu^{3+} present in the hole-doped cuprate $\text{La}_{2-x}\text{Sr}_x\text{CuO}_4$. However, there are many examples where this classification is not valid—Fe in FeS_2 for example is actually $2+$ and there are accordingly missing sulfur $3p$ electrons. This leads to the formation of sulfur pairs having a net pair valence of $2-$ rather than $4-$. In this case the antibonding S $3p$ states in the pairs are empty and therefore form rather narrow bands just above the chemical potential which form the conduction band (depending on where the transition-metal electron addition d states are, as we will discuss below). Similarly, in superoxides such as KO_2 the O atoms form pairs, but now with each pair having a $1-$ charge and spin of $1/2$, leading to an O $2p$ hole-based ferromagnetic ground state. In the hole-doped cuprates, convention would predict the introduction of Cu^{3+} into the mainly Cu^{2+} lattice, leading to a mixed valent state. However, it is known that the holes actually reside mainly in O $2p$ orbitals, leaving the Cu with a $2+$ valence and a spin of $1/2$. In some pictures (like that of the Zhang-Rice singlets) these O holes tend to form molecules of 4 oxygen atoms in a square around a particular Cu, forming a singlet spin state due to the very strong Cu-O exchange interaction which is of order 0.5 eV. Similarly, we will argue that also Ni does not really like to be $3+$ and so in the perovskite structure rare-earth nickelates the Ni behaves like Ni^{2+} in a normal high-spin state of $S = 1$ and there is one hole per 3 oxygens in the O $2p$ band of states. Realizing that each Ni is at the center of an octahedron of O ions we would have on average 2 holes per O octahedron and again these are found to condense into octahedral molecules of O around every second Ni^{2+} ion.

In this lecture we will look at the consequences for the electronic structure and the corresponding physical properties of oxides involving unconventionally high cation oxidation states which accordingly may better be viewed as having unfilled anion valence bands. In solid state physics we are mostly interested in the low-energy scale possible excitations from the ground state which determine the physical properties in a temperature range of perhaps 0 to 500 K, thus we

will focus our considerations on those states which are at most several eV above and/or below the chemical potential. Further, in the study of transition-metal oxides or rare-earth compounds we mostly start from a viewpoint of what the valences of the elements are in the limit of zero interatomic hybridization (i.e., in the ionic limit). The hybridization, which of course plays a crucial role, is then introduced and band structures and interatomic interactions result. As we know, in transition-metal based ionic solids the valence state of an ion determines the number of d electrons involved and this in turn determines the spin, orbital, and total angular momentum via Hund's rules in the lowest energy states. The excited states, or multiplets, important in describing various forms of spectroscopy are also determined to first order in this ionic starting point. Thus, this starting knowledge is the first guess as to what the spin and the d occupation numbers really are in the material. However, if indeed the anion valence states are not fully occupied and the cations accordingly have unexpected valences in the ionic limit, the lowest energy states could be very different from this formal oxidation state based picture, and the model Hamiltonians which should be used could differ strongly from the typical ionic ansatz. This is especially important for the analysis of materials using x-ray based spectroscopies such as resonant x-ray reflectometry and resonant elastic and inelastic x-ray scattering.

In the following we will start with a brief motivation of the importance of anion states by looking at divalent late $3d$ transition-metal (i.e. Ni or Cu) oxides. We will discuss how studies of the first ionization states found that doped holes were more likely to occupy the ligand (oxygen) states. From this introduction we will then look at higher valence oxides where holes can be *self-doped* into the ligand band. We will show how this affects the usual crystal field and Hund's rule based starting points of a typical theoretical model. In Section 3, we will then progress to the very basic classification scheme referred to as the ZSA scheme, which did not focus on the case of very high oxidation states for which the so called charge-transfer gap could be negative. We will discuss the various classes possible in an extended ZSA scheme, showing the transition from Mott-Hubbard to charge-transfer to mixed-valence and then to the strong negative charge-transfer gap systems. In each case we look at the ground state and the electron removal and addition states (i.e., the one-electron Green functions). In Section 4, we will look at examples of very interesting negative charge transfer compounds, including the perovskite nickelates and also the related non-correlated bismuthates. Here we will also show how a significant amount of information concerning the ground state local electronic structure can be obtained from resonant x-ray absorption and scattering experiments, and will introduce the model Hamiltonians which can be used in this regard. Lastly, in Section 5 we will look at materials in the fascinating mixed-valence class, focusing primarily on the highly studied samarium hexaboride.

2 The importance of anion states

In this section, we will provide some generally accepted examples which exemplify the importance of anion states in high-valence oxides. First we will give a brief review of the studies of hole-doped states in divalent copper and nickel oxides which led to the concept of Zhang-Rice singlets in the high- T_c cuprates. Following that we will show that similar effects can be

present in undoped compounds with high formal oxidation states, such as Ni^{3+} in the perovskite rare-earth nickelates.

2.1 Hole doped states in divalent Cu and Ni oxides

The common feature among all high- T_c cuprate compounds are the CuO_2 planes (containing Cu^{2+} in the parent compounds) which are doped with holes or electrons to induce superconductivity. Of critical importance then, when trying to understand the nature of high- T_c , is to understand the nature of the doped carriers. Early spectroscopic studies, particularly x-ray absorption spectroscopy (XAS) at the oxygen K edge, found strong evidence that the holes doped into CuO_2 planes primarily resided in the oxygen $2p$ band [1–3]. This showed that the doping did not yield Cu^{3+} in the lattice, and accordingly that the Cu was still $2+$ with $S = 1/2$.

Theoretical studies were undertaken to understand the character of the doped holes. In particular, an Anderson impurity model was employed by Eskes *et al.* to examine the one-electron removal spectrum of a Cu^{2+} impurity which hybridized with an oxygen $2p$ band, as this spectrum relates directly to the states achievable through hole doping [4]. It was found that since the Cu d^8 states were below the top of the O $2p$ band (i.e., the parent compound is a charge-transfer insulator) the first ionization state is a singlet $^1A_{1g}$ state which is pushed out of the O $2p$ continuum. Around the same time, the similar Zhang-Rice (ZR) singlet picture was developed [5], which is also based on the fact that the doped holes occupy linear combinations of oxygen $2p$ orbitals in a square coordinated around the Cu site.

These early studies of the cuprate superconductors showed the importance of the anion states, especially upon doping. However, even with this importance established, there are very different ways in which the anion states can be treated. On one hand, the ZR singlet picture was rather quickly adopted by many working on the theory of high- T_c cuprates, in part because it simplifies the problem to that of an effective single-band Hubbard model where the charge-transfer energy plays the role of U . Due to the extended nature of the “atomic” wave function, which includes the linear combination of O $2p$ orbitals of $x^2 - y^2$ symmetry, longer-range hoppings beyond nearest neighbors have to be included. A large number of theoretical studies have been carried out and still use this single-band approach. On the other hand, also at the very beginning of the field in 1988, Emery and Reiter [6] introduced a somewhat different model also based on doped holes being mainly on O but placing the importance of the holes on the very large antiferromagnetic exchange interaction of the O $2p$ hole with its *two* neighboring Cu spins. This leads to the description of the quasiparticle as being a three-spin polaron. Recently, this model has gained considerable support from a very large scale exact diagonalization study by Lau *et al.*, who found that the ground state and k dependence of the single hole in the full 3-band model is in close agreement with the 3-spin polaron model in which a strong Cu-Cu ferromagnetic correlation is found for the Cu atoms sandwiching the O $2p$ hole [7–9]. Another interesting part of this calculation is also that, without introducing longer-range hoppings, it yields basically the same dispersion relation for the quasiparticle as the extended single-band Hubbard model, although the spectral weights differ considerably. The ferromagnetic correlation of the neigh-

boring Cu spins to the O hole is something that seems difficult to reconcile within a single band Hubbard model based on ZR singlets. It is also interesting to note that in recent work it has been shown that different models giving basically the same single particle dispersion can yield very different two particle spectral functions as are relevant for superconductivity [10]. Thus, debate remains regarding the importance of the explicit inclusion of the anion states in models describing the cuprates.

In addition to the identification of doped holes in cuprates occupying O $2p$ orbitals, similar studies showed that when NiO is hole-doped with Li, the holes also occupy the oxygen $2p$ orbitals [11]. For Li-doped CoO, the holes have a strongly mixed Co $3d$ and O $2p$ character [12]. Given that all of these parent compounds are divalent, one should expect the anion states to become even more important in higher valence oxides, where charge-transfer energies are generally smaller due to increased electron affinities of the metal ions.

2.2 Similar effects in undoped negative charge transfer compounds

The previous section detailed the importance of oxygen $2p$ holes in hole-doped divalent late $3d$ transition-metal oxides. In this section we will introduce how such oxygen holes may be present in *undoped* high-valence oxides due to the presence of a so-called negative charge transfer energy. To accomplish this, we first provide a brief example in Figure 1(a) of how crystal field and Hund's rule energetics determine the ground state configuration of a correlated transition-metal ion in a compound. For this example of a Ni^{3+} ion, first one accounts for multiplet interactions. According to Hund's first rule, we assume our lowest energy configuration is the one with maximum spin. The next highest state we consider has one spin flipped, which in this case costs energy $2J$, where $J = \frac{1}{14} (F^2 + F^4)$, and F^2 and F^4 are the multipole Coulomb (Slater) integrals [13,14]. Next, we account for an octahedral crystal field potential, which splits the $3d$ orbitals into an e_g group and a t_{2g} group. Evident from this picture is that depending on the relative sizes of J and $10Dq$ (where $10Dq$ is a measure of the point charge crystal field [15]), one can have either a high-spin or low-spin ground state.

In Fig. 1(b), we now extend our example to a configuration interaction (CI) model. Now we explicitly account for hybridization with nearest neighbors. Assuming the neighbors are fully occupied ligands, with CI one constructs a wavefunction out of a linear combination of configurations of the form $d^{n+i} \underline{L}^i$, where $i = \{0, 1, 2, \dots\}$ and \underline{L} is a hole in the ligand shell left behind when an electron hops to the $3d$ shell. Note that the ligand hole orbital must have the same symmetry as the central d ion. The energy cost of a ligand electron transferring to the d shell is the charge-transfer energy Δ , and one must also account for additional Coulomb energies when extra electrons hop to the d shell. If we set the energy of the $d^n \underline{L}^0$ (i.e. $i = 0$) configuration to 0, then the energies of the $i = 1, 2, 3, \dots$ configurations are given by Δ , $2\Delta + U$, $3\Delta + 3U$, and so on.

Returning to Fig. 1(b), here we analyze possible positive and negative charge-transfer cases for formally trivalent Ni^{3+} oxides using a simplified configuration interaction model. Starting with $3d^7$ and $3d^8 \underline{L}$ configurations (where \underline{L} denotes a ligand hole), we show the configuration

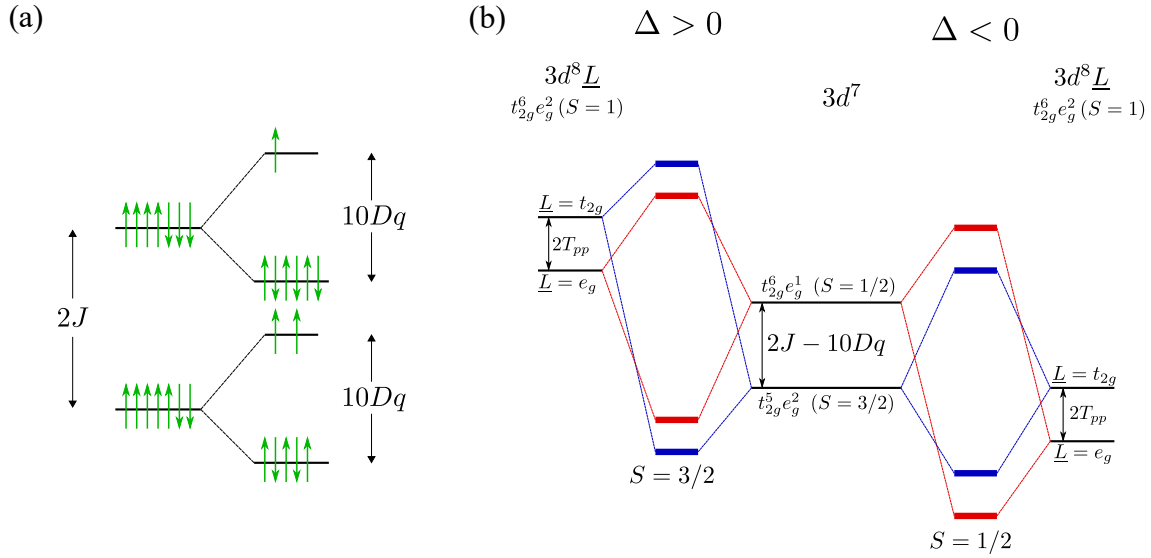


Fig. 1: (a) The Hund's rule and crystal field energetics are introduced for a Ni^{3+} (d^7) system. (b) A configuration interaction model demonstration why low-spin Ni^{3+} compounds must be negative charge transfer systems. For $\Delta > 0$ (left), typical hopping integrals are not strong enough to push the low-spin bonding state below the high-spin bonding state. For $\Delta < 0$ (right), however, the low-spin state is easily stabilized as the ground state.

interaction bonding and antibonding states for positive (left) and negative (right) charge transfer situations. The $3d^7$ configuration has two states in this simplified picture which are the high-spin ($S = 3/2$, $t_{2g}^5 e_g^2$) and low-spin ($S = 1/2$, $t_{2g}^6 e_g^1$) states. The energy separation between the states before hybridization is considered is given by $2J - 10Dq$ where J is approximately 1.25 eV (according to atomic Hartree-Fock calculations [14], rescaled by 80% to account for intra-atomic configuration interaction as usual) and the point-charge crystal-field contribution $10Dq$ is roughly 0.75 eV (slightly larger than the ~ 0.5 eV usually used for divalent compounds, to account for the shorter bond lengths in formally trivalent compounds). Each of these states hybridizes with the $3d^8 \underline{L}$ configuration, where the d electrons have a high-spin ($S = 1$, $t_{2g}^6 e_g^2$) arrangement. The ligand hole consists of a linear combination of O $2p$ orbitals of π or σ bonding symmetry with the transition-metal $3d$ orbitals. Thus, the hole can be of e_g or t_{2g} symmetry, yielding two states separated by $2T_{pp} = (pp\sigma - pp\pi) \approx 1.5$ eV [16].

When hybridization is gradually introduced for this positive charge transfer case, a bonding $S = 3/2$ ground state is attained, illustrated by the lower blue line in the figure. Given that the e_g hopping integral is generally about twice as large as the t_{2g} for octahedrally coordinated transition-metal compounds, one would expect that for increased hybridization strength the low-spin (red, $S = 1/2$) bonding state would eventually become the ground state. However, such a situation would require significantly larger hopping integrals than are present in the $3d$ oxides.

If instead we consider the negative charge transfer arrangement of our configurations as shown on the right of Fig. 1(a), a low-spin state arises much more naturally. Now the $d^8 \underline{L}$ states are below the d^7 , and when hybridization is introduced the bonding state having the symmetry of

the $t_{2g}^6 e_g^1$ configuration and thus with ($S = 1/2$)—but with mainly $d^8 \underline{L}$ character—is stabilized as the ground state. Thus by having a negative charge-transfer energy and accordingly a strong ligand-hole contribution to the ground state, a low-spin Ni compound is realized with typical hopping integrals. One can consider this as a competition between the Hund’s rule J , which wants to maximize the spin, and the O $2p$ – TM $3d$ exchange interaction which is antiferromagnetic. If the hole is mainly on the oxygen rather than in a t_{2g} orbital of the (d^7) Ni, then it would rather be in an e_g symmetry state and would have a strong antiferromagnetic coupling with the d^8 spin-1 state, leading to a $S = 1/2$ state. Note that with a negative charge transfer energy, the stronger e_g hybridization leads to a unique inverted contribution to ligand-field splitting from covalence [17].

In Fig. 2(a), we test this simplified picture using a full configuration interaction calculation for a NiO_6 cluster having Coulomb interactions, crystal-field, spin-orbit, and ligand-ligand hopping energies characteristic of the perovskite rare-earth nickelates, $R\text{NiO}_3$. The black solid line shows the low-spin/high-spin transition as a function of the effective charge-transfer energy Δ_{eff} and the hybridization strength V_{e_g} (with $V_{t_{2g}}$ fixed at $0.58 V_{e_g}$). Here, Δ_{eff} accounts for the various energy shifts of the multiplet Coulomb interactions, ionic crystal-field contribution, spin-orbit interaction, and T_{pp} , such that with no hybridization the lowest-energy $d^8 \underline{L}$ state crosses below the lowest-energy d^7 state when Δ_{eff} becomes negative. The color of the plot indicates the contributions of the d^7 and $d^8 \underline{L}$ configurations to the ground state (note the basis also contains $d^9 \underline{L}^2$ and $d^{10} \underline{L}^3$ configurations, so we plot the *relative* weights of the d^7 and $d^8 \underline{L}$ for clarity).

A key observation from Figure 2(a) is that the low-spin regime is always characterized by a dominant $d^8 \underline{L}$ contribution to the ground state. This includes a sharp jump in $d^8 \underline{L}$ weight at the spin-state transition, originating from the fact that the hybridization is stronger for the low-spin states which have more e_g holes. The phase diagram confirms the discussion of Figure 1(b)—that a low-spin state can be achieved with realistic hybridization parameters if the ground state is mainly $d^8 \underline{L}$ —and actually shows that even for very large hopping integrals the low-spin state is still mainly $d^8 \underline{L}$. Note that the ground state can have more $d^8 \underline{L}$ than d^7 character even for $\Delta_{\text{eff}} > 0$ as the $d^9 \underline{L}^2$ and $d^{10} \underline{L}^3$ configurations push the $d^8 \underline{L}$ lower in energy than the bare charge-transfer value Δ_{eff} . We also indicate with the star in Fig. 2(a) the location of the rare-earth nickelates in this phase diagram. For these parameters [18], the nickelates are indeed best described as negative charge transfer compounds. We will discuss the nickelates further in Section 4.

For clarity, in Fig. 2(b) we demonstrate the relationship between the typically used Δ , and Δ_{eff} which is more relevant for small and negative charge transfer energy systems. Within our configuration interaction scheme, Δ defines the central energies of the various configurations. As displayed in the figure and explained in the caption, configurations with n ligand holes have energy $n\Delta$, with an additional energy-offset due to the Coulomb repulsion U . However, within each configuration are multiplet, crystal-field, spin-orbit, and ligand-ligand hopping (T_{pp}) energies, which mean that the lowest state within each configuration will be shifted from the central energy by different amounts. One should then define the energy Δ_{eff} , which is the energy be-

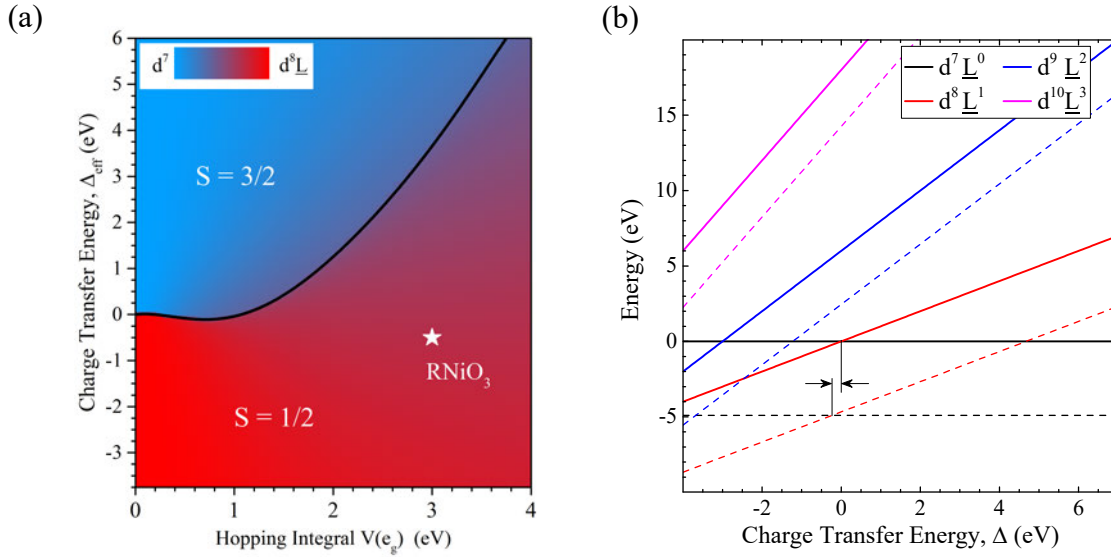


Fig. 2: Results of a full configuration interaction calculation. (a) The low-spin phase space is always characterized by a dominant $d^8 \underline{L}$ component in the ground state wavefunction. (b) Solid lines show the shell average energies, given by 0 , Δ , $2\Delta + U$, and $3\Delta + 3U$ for the d^7 to $d^{10} \underline{L}^3$ configurations, respectively. The dashed lines are the lowest multiplet for each configuration, which account for higher multipole Coulomb interactions, crystal fields, spin-orbit interactions, and T_{pp} . The arrows show the difference between the configuration averaged Δ (used for the x axis), and the effective charge-transfer energy Δ_{eff} , which becomes negative when the lowest energy $d^8 \underline{L}$ multiplet is lower than the lowest d^7 multiplet.

tween the lowest energy d^7 state and the lowest energy $d^8 \underline{L}$ state. For the case of Fig. 2(b), the difference between Δ and Δ_{eff} is relatively small, but for other elements and d shell fillings, the difference can be significantly larger.

3 Classification of correlated compounds

3.1 Mott-Hubbard and charge-transfer insulators

It has been known for many years that often correlated transition-metal compounds such as NiO or CoO have substantial electronic band gaps of a few eV, whereas band theory predicts much smaller gaps or no gaps at all [19]. The explanation for this discrepancy came from the ideas of Mott and Peierls [20, 21], and relies on the fact that the $3d$ electrons forming states near the Fermi level are relatively localized, and therefore have large Coulomb repulsion energies, denoted by U . This U then suppresses charge fluctuations of the form $d^n d^n \rightarrow d^{n-1} d^{n+1}$ which would describe the conduction in such a material. Formalizing these ideas into a suitable model led to the development of the Hubbard model [22, 23] and such materials are accordingly often termed Mott-Hubbard insulators. A simplified illustration of the effect of the Coulomb repulsion U on an otherwise metallic $3d$ density of states is shown in Fig. 3(a), where a broad metallic band splits into a full lower band and empty upper band with an insulating gap determined by

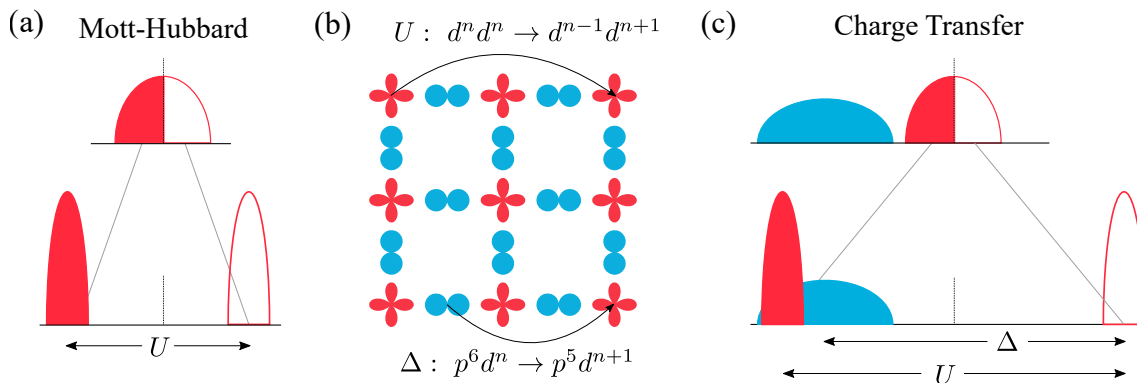


Fig. 3: Distinction between Mott-Hubbard and charge-transfer insulators introduced by the ZSA work. (a) A broad, metallic band is split into full and empty electron removal and addition bands by Coulomb repulsion, and leads to an insulating gap of size U . (b) The low-energy charge fluctuations of energies U and Δ are illustrated. The red orbitals correspond to correlated transition-metal sites while the blue are those of the ligands. (c) The concept of a charge-transfer insulator, where the gap now involves the ligand states and is determined by Δ , which can be much smaller than U .

the size of U . Figure 3(b) demonstrates the type of charge fluctuation in a correlated compound which costs energy U .

While this Mott-Hubbard understanding of correlated insulators was enormously successful, some new issues arose when applying it to various materials. It was found, for example, that the size of U in materials like NiO (~ 7 eV) is actually quite a bit larger than the electronic band gap (~ 4 eV), and thus it was evident that something else must be at play to determine the gap. Additionally, among series of such materials, the size of the gap often correlates more directly to the anion electronegativity than to the cation U . In fact, many sulfides which should have comparable U values to oxides are actually conductors. Further, new experiments and configuration interaction based interpretations in the mid 1980s found that the first ionization state of NiO had largely oxygen $2p$ character, and not the expected lower Hubbard band ($d^8 \rightarrow d^7$) character [24, 25].

As a solution to these discrepancies, the Zaanen-Sawatzky-Allen (ZSA) theory of correlated compounds was developed [26]. By using an Anderson impurity model applicable to such insulating compounds, the ZSA study found that in many compounds U is not the important energy scale for the band gap, but rather the charge-transfer energy Δ . The charge-transfer energy is defined as the energy cost of removing a ligand (i.e. oxygen, sulfur, etc.) $2p$ electron and placing it in a transition-metal $3d$ orbital. A schematic density of states (in the limit of no metal-ligand hybridization) is shown for a charge-transfer compound in Fig. 3(c). Again the upper part of the Figure shows the DOS without Coulomb interactions considered, this time now with the $3d$ band in red and a fully occupied ligand $2p$ band in blue. In the lower part, the Coulomb repulsion is included, leading to the formation of upper and lower Hubbard bands. Now one can see that if Δ is smaller than U , the lower-energy charge fluctuations which determine the energy gap of the compound will be of the form $p^6 d^n \rightarrow p^5 d^{n+1}$, where p refers

to the ligand $2p$ orbitals as shown in Fig. 3(b). The ZSA scheme led to a very comprehensive understanding of the conductivity behavior of many classes of transition-metal compounds [26]. In particular it is the early transition-metal oxides, such as V_2O_3 , Ti_2O_3 , Cr_2O_3 , etc., which can be described as Mott-Hubbard insulators, while the later $3d$ oxides like CoO, NiO, and CuO are charge-transfer insulators.

3.2 Mixed valence and negative charge transfer insulators

While the original ZSA theory provided a sound qualitative understanding of many transition-metal compounds, it did not focus much on compounds with high oxidation state cations. Generally, for increased cation oxidation states while keeping the anions fixed, one expects a decrease in the charge-transfer energy as the electron affinities of the higher valence states are larger. In Fig. 4, we show schematic electron addition and removal spectra, in the limit of vanishing metal-ligand hybridization, as the charge-transfer energy is gradually reduced from the Mott-Hubbard regime to the charge-transfer regime and further. We have a broad band (shown in blue) due to the light electrons (ligand $2p$) and narrow Hubbard bands (red) for the correlated electrons (metal $3d$). The Hubbard bands are again separated by the Coulomb repulsion energy U , and the energy separation between the center of the upper Hubbard band and the center of the light-electron band is again defined as the charge-transfer energy, Δ . This definition of Δ is the most common [26], but we also define an effective charge-transfer energy Δ_{eff} between the top of the broad band and the bottom of the upper Hubbard band. This effective charge-transfer energy is more relevant when describing high oxidation state compounds. When higher multipole Coulomb interactions (multiplets) are included, Δ_{eff} would also account for these, and would be the energy difference between the lowest (i.e. Hund's rule) d^n state and the lowest $d^{n+1}\underline{L}$ state. In our simple schematic, which neglects multiplet effects, we can relate Δ and Δ_{eff} as

$$\Delta_{\text{eff}} = \Delta - \frac{w_d + w_p}{2} \quad (1)$$

where w_d and w_p are the widths of the metal and ligand ($3d$ and $2p$) bands. If multiplets are included, one should use the strict definition of Δ_{eff} as the energy difference between the lowest d^n and $d^{n+1}\underline{L}$ multiplets.

As the charge-transfer energy is reduced moving downward in Fig. 4, four distinct regimes are encountered. The first two are the Mott-Hubbard and charge-transfer regimes, as discussed above in relation to the ZSA work. However, if one continues to reduce the charge-transfer energy, the mixed-valence phase is reached. Here the d^{n+1} original upper Hubbard band has now crossed into the top of the valence band. As indicated, the ground state becomes more difficult to represent, with some atoms in a d^n and some in a d^{n+1} configuration, leading to lower and upper Hubbard bands of d^{n-1} and d^{n+2} , respectively, which are separated by a total energy of $2U$. The now very complicated ground state wavefunction depends on details of longer-range interatomic interactions, which may lead to a kind of ordering of the transition-metal valence states. An example is the case of magnetite (Fe_3O_4), where in the spinel structure the tetrahedral

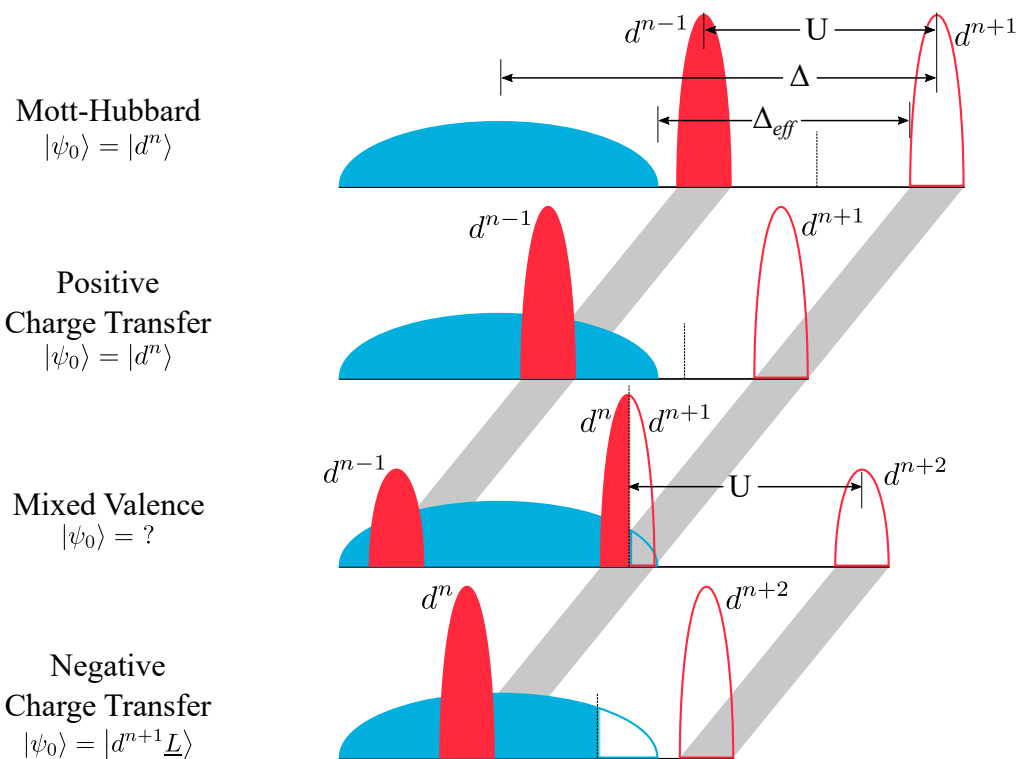


Fig. 4: The energetics of correlated compounds depicted with schematic electron removal and addition spectra. A broad band, nominally full, is shown in blue and narrow, correlated (d) bands are shown in red. A very small hybridization is assumed between the broad and narrow bands. A constant Coulomb repulsion U separates lower and upper Hubbard bands throughout the figure, whereas the charge-transfer energy Δ is varied. The Fermi level is shown with a dashed vertical line and electron removal spectra are shaded in, while electron addition spectra are only outlined. Moving from the top to bottom, the energy of the correlated bands is shifted lower, leading to a reduction of the charge-transfer energy and the four distinct regimes. The nature of the ground state wavefunction $|\psi_0\rangle$ is given for each case.

sites contain Fe^{3+} but the octahedral sites are mixed valent (though not due to a negative charge-transfer gap), and below the so-called Verwey transition some kind of charge ordering occurs which is not yet clearly resolved [27, 28]. Such charge density wave like situations can indeed involve multiple \mathbf{q} vectors and form complicated structures. Additional examples are doped LaMnO_3 and other doped transition-metal compounds. In Section 5 we will consider a case of very small hybridization in SmB_6 where a unique, new form of ordering of the valence in momentum space rather than real space is suggested.

Moving beyond the mixed valence regime in Fig. 4, by decreasing the charge-transfer energy further we enter the negative charge transfer phase. Here the ground state is described as $|d^{n+1}\underline{L}\rangle$ meaning that the upper and lower Hubbard bands are now d^{n+2} and d^n states, respectively, where again n is the filling which corresponds to the formal valence. The ligand band has now been accordingly *self-doped* [29, 30] with holes. In other words, this regime corresponds to the case where a transition-metal cation does not adopt its formal oxidation state, instead keeping one extra electron which leaves the anion with one fewer. Generally electron affinities

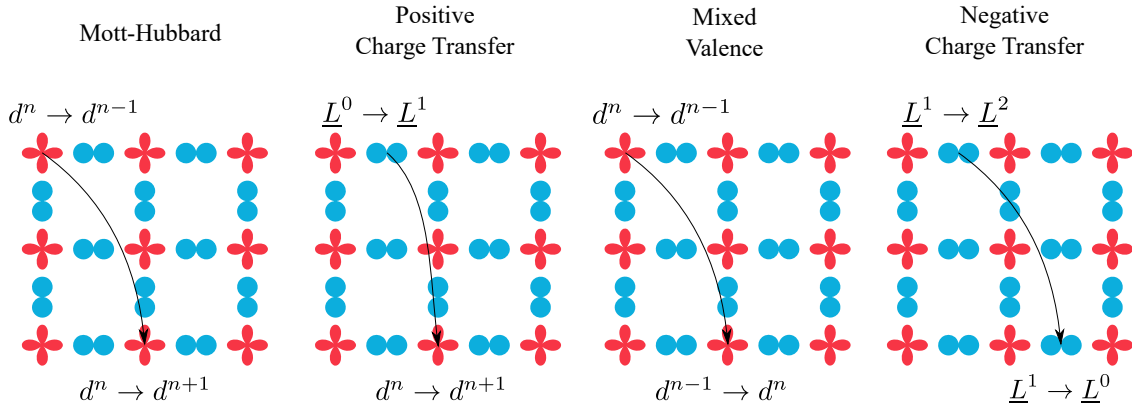


Fig. 5: Lowest energy charge fluctuations in the different classes of correlated compounds.

increase moving toward the end of the $3d$ series and, as mentioned above, with increasing cation valence. Thus it is expected that formally trivalent Ni^{3+} and Cu^{3+} oxides, as well as formally tetravalent oxides of Co^{4+} and Fe^{4+} , will be in the negative charge-transfer regime, or at least mixed valent. One can also move toward the negative charge-transfer regime via ligands with weaker electronegativities. Thus going from oxides to sulfides or selenides (or from fluorides down to iodides) will generally move one closer to, or into, the negative charge-transfer regime. In Fig. 5, we extend the schematic charge fluctuations of Fig. 3(b) to now include the mixed valent and negative charge-transfer classes. As before, the Mott-Hubbard and positive charge-transfer classes are characterized by lowest energy charge fluctuations determined by U and Δ , respectively. Mixed valent compounds are typically metals or have very small gaps, with charge fluctuations that can involve both the cation and anion states. In the limit of very small hybridization, however, very interesting charge fluctuation behavior can occur, as we will discuss in the context of SmB_6 in Section 5. Negative charge-transfer compounds have a metallic ligand $2p$ DOS before the inclusion of hybridization, and so may be (bad) metals, or may have many different behaviors, including metal-insulator transitions as in the rare-earth nickelates.

4 Negative charge transfer compounds

As alluded to in the previous section, in general the conditions favorable for negative charge-transfer energies are large electron affinities on the cations, achievable through high formal valences and cations near the end of the $3d$ series, and low ligand electronegativities, achievable by going from halides to chalcogenides to pnictides, or moving down the respective columns of anions in the periodic table. In this section, we will look at some example materials in detail.

4.1 Perovskite rare-earth nickelates

The perovskite rare-earth (R) nickelate compounds, $R\text{NiO}_3$, exhibit many fascinating properties including a metal-insulator transition, with temperatures tunable via the size of the rare-earth

ion [31]. In the insulating phase, the nickelates undergo a structural distortion where alternating NiO_6 octahedra expand and compress in a rocksalt pattern breathing distortion. Additionally, within this insulating phase the nickelates also order antiferromagnetically with an unusual $\mathbf{q} = (1/4, 1/4, 1/4)$ propagation vector. First synthesized in the 1970s [32], the nickelates rose in popularity through the early 1990s [33–35], and are extremely popular today as they are a prime example of how emergent properties can be tuned through heterostructured growth [36–40].

The nickelates have a formal Ni^{3+} oxidation state, suggesting a $3d^7$ occupation of the nickel. Various studies have indicated that the nickelates possess a low-spin state, so early interpretations were that the ground state had a $t_{2g}^6 e_g^1$ occupation, with $S = 1/2$. However, such a state should have a strong Jahn-Teller effect similar in strength to that observed in Mn^{3+} perovskite oxides like LaMnO_3 , but one is not observed experimentally. Additionally, one has the arguments laid out in Section 2, which showed that low-spin Ni^{3+} oxides should be very rare if not impossible. With these key observations established, it has become clear in recent years that the nickelates are actually negative charge-transfer compounds with a ground state better described as $3d^8 \underline{L}$ (though with a certain d^7 contribution to the wavefunction due to strong hybridization) and with a $S = 1/2$ spin that emerges from antiferromagnetic coupling between a $t_{2g}^6 e_g^2$ ($S = 1$) configuration and a self-doped ($S = 1/2$) ligand hole.

When viewed as negative charge transfer materials, the metal-insulator transition and unique magnetic ordering of the nickelates can be understood on a theoretical basis. As shown by Mizokawa *et al.* [41], and later by others [42,43], when the negative charge-transfer $d^8 \underline{L}$ ($S = 1/2$) ground state undergoes the breathing distortion, a traditional $3d$ -based charge disproportionation does not occur. Instead, a *bond* disproportionation occurs, and the distinct expanded and compressed NiO_6 octahedra take on respective configurations tending toward $d^8 \underline{L}^0$ ($S = 1$) and $d^8 \underline{L}^2$ ($S = 0$). The situation then appears to instead resemble Peierls type of physics, involving strong electron-phonon interactions.

Recently we have adapted these negative charge-transfer theories to models which can be applied to the analysis of resonant x-ray spectroscopy experiments. Conventional approaches to the analysis of various core-level absorption, photoemission, and scattering data include multiplet ligand-field theory and the multiplet Anderson impurity model. In the former, a MO_6 cluster is analyzed using configuration interaction theory, including all Coulomb interactions of the $3d$ and relevant core shells, and hybridization with the nearest neighbor ligands is included. In the impurity approximation, hybridization with a bath of ligands is included, instead of just the nearest neighbors, to account for the ligand bandwidth. These two techniques have had great success in the analysis of core level spectra for the $3d$ oxides (see, e.g. [44–46]). However, these approaches were never successful in modelling the various spectra measured on rare-earth nickelates.

Key x-ray spectroscopy experiments on the nickelates include x-ray absorption spectroscopy (XAS), resonant magnetic diffraction (RMD), and resonant inelastic x-ray scattering (RIXS). First, the oxygen K -edge XAS spectra show a strong pre-edge feature [47], indicative of a large hole character in the oxygen $2p$ orbitals, which can be viewed as evidence for negative charge-transfer energetics. The XAS spectra at the Ni $L_{2,3}$ edge are characterized by a strong, sharp first

peak, followed by a broader continuum-like feature [48, 49]. Earlier studies using a multiplet ligand-field theory (MLFT) approach to interpret these XAS lineshapes showed some success with interpreting the primary features as different multiplet peaks arising from a highly mixed final state spectrum [50]. However, such an interpretation has now been found to be inconsistent with the lineshapes of RMD spectra, where the magnetic response is heavily concentrated at the energy of the first sharp XAS peak. In fact, most models to date could obtain a certain degree of agreement with the lineshapes of either XAS or RMD, but not both.

The conventional ligand-field theory (or cluster model) used for $L_{2,3}$ edge spectroscopy, and employed for most previous studies on the nickelates, has the Hamiltonian:

$$H_{LF} = H_U^{dd} + H_U^{pd} + H_{l,s}^d + H_{l,s}^p + H_o^p + H_o^d + H_o^L + H_{hyb}^{dL}, \quad (2)$$

with,

- H_U^{dd} the Coulomb repulsion between two $3d$ electrons including all multiplet effects,
- H_U^{pd} the Coulomb repulsion between a $2p$ core and $3d$ valence electron including all multiplet effects,
- $H_{l,s}^d$ the $3d$ spin-orbit interaction,
- $H_{l,s}^p$ the $2p$ core level spin-orbit interaction,
- H_o^p the onsite energy of the $2p$ core orbitals,
- H_o^d the orbital dependent onsite energy of the $3d$ valence orbitals,
- H_o^L the orbital dependent onsite energy of the Ligand orbitals, and
- H_{hyb}^{dL} the hybridization strength between the $3d$ and Ligand orbitals.

The onsite energies account for the specific charge-transfer energetics of the system. Detailed expressions for each term can be found elsewhere [18]. This model can be adapted to the breathing-distorted nickelates by moving to a double cluster model, where two Ni-O octahedra represent the expanded and compressed octahedral sites of the nickelate lattice. One then has the Hamiltonian

$$H = H_{LFA} + H_{LFB} + H_{mix} \quad (3)$$

where H_{LFA} and H_{LFB} are complete ligand field theory Hamiltonians of the compressed and expanded sites, and H_{mix} adds hybridization between them. Realizing that the rocksalt distortion means the two octahedra types are arranged in an O_h symmetric manner, H_{mix} consists of hybridization operators having e_g and t_{2g} symmetry [18].

With this model for the local electronic structure, a two site arrangement is created which does not break the O_h point group symmetry, and both the negative charge transfer self doping and the bond disproportionation physics can be captured. Importantly, with such a model all of the $3d$ orbitals are in the basis (as opposed to the earlier restricted orbital studies [41–43]) and the core orbitals are also in the basis, so accurate spectroscopy simulations can be performed. The effects of negative charge transfer and bond disproportionation can then be compared against experiment.

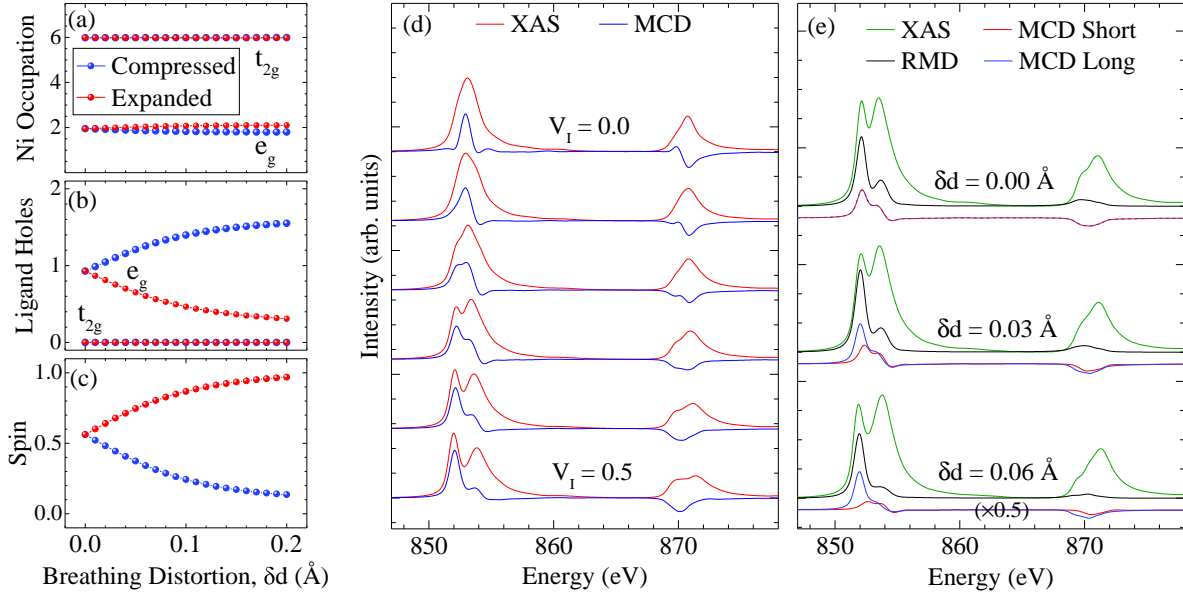


Fig. 6: Ground state characteristics and spectral responses of perovskite nickelates from a double cluster model. (a-c) The Ni (a) and ligand (b) occupations show that the breathing distortion involves primarily the oxygen 2p holes rather than the Ni 3d electrons. (c) The spins on the long and short bond Ni tend toward $S = 1$ and $S = 0$, respectively. (d) The single cluster limit ($V_I = 0$) cannot reproduce the two-peaked structure at each edge with MCD focused on the first peak, but with $V_I > 0.3$ these features are captured by the double cluster. (e) A breathing distortion splits the XAS peaks further, and the magnetic diffraction signal is focused at the energy of the first XAS peak, both in agreement with experiment.

In Fig. 6(a-c), we detail the ground state properties of the double cluster model, as a function of the size of the breathing distortion. The results confirm those of the previous restricted orbital studies—under the breathing distortion, very little charge disproportionation occurs via the 3d electrons, whereas the ligand holes are rather active. With no breathing distortion each octahedron has a $3d^8\bar{L}$ configuration, but as shown in Fig. 6(b) in the presence of the breathing distortion the holes bond more strongly with the short bond Ni than the long bond. This leads to a reduction of the spin moment on the compressed octahedron, such that it tends toward $S = 0$ while the expanded octahedron tends toward $S = 1$ (Fig. 6(c)).

In Fig. 6(d), we show calculated Ni $L_{2,3}$ XAS spectra for different values of intercluster hopping V_I [18], starting from the conventional single cluster limit ($V_I = 0$). In the single cluster limit, the spectrum looks very different from experiment [48, 49], as the characteristic two peak structure for the L_3 resonance near 853 eV is completely missing. However, for increasing V_I to 0.3 and higher, a pronounced first peak is pushed out of the resonance, and the spectra strongly resemble experiment. Thus it is evident for such a highly covalent, negative charge-transfer energy compound that intersite interactions not captured in single cluster models are very important in the spectral response. Additionally, one can see that the fundamental magnetic circular dichroism (MCD) response is strongly concentrated at the first sharp peak, which is a crucial requirement for agreement with magnetic scattering experiments.

In Fig. 6(e) we show the XAS, MCD, and resonant magnetic diffraction (RMD) responses for three different sizes of lattice breathing distortions, δd . First, we see that for increasing breathing distortion, the total XAS spectral shape (summed over the two sites) only changes a minor amount, with the two L_3 peaks moving apart with increased breathing distortion. This trend is in good agreement with the rare-earth series, where smaller rare earths lead to larger breathing distortion and slightly more separated XAS peaks [48, 49]. Next, we note that the MCD spectra of the two sites become inequivalent when the breathing distortion is introduced. In accordance with the different spin moments for the two Ni, the long bond MCD spectrum becomes stronger and the short bond becomes weaker. However, the strongest response is always at the energy of the first XAS peak. This leads to the distinct RMD spectral shapes as shown, which again are strongly peaked at the first XAS resonance. This characteristic agrees very well with all experiments on various nickelate bulk and heterostructure materials.

The double cluster model thus bridges the gap between the recent theories of bond disproportionation in the nickelates [41–43], and experimental observations made through spectroscopy. The key aspect of the model is the inclusion of the full $3d$ orbital degeneracy, as well as the $2p$ core shell, which allows the simulation of core level spectroscopy. The excellent agreement between the calculated and experimental XAS and RMD provides validation for both the negative charge-transfer energy and bond disproportionation theory of the nickelates.

4.2 Perovskite bismuthates

Up until this point, our focus has been on correlated transition-metal compounds. However, it has recently been shown that the non-correlated perovskite bismuthates SrBiO_3 and BaBiO_3 exhibit characteristics very similar to the negative charge transfer picture discussed above [51]. These compounds, when doped, are high- T_c superconductors and have accordingly attracted significant attention. Interestingly, at low temperatures they exhibit the same breathing type of lattice distortion that was introduced above for the nickelates. Every other octahedron expands or compresses in a rocksalt-pattern distortion. Earlier studies suggested that the breathing distortion was concomitant with a charge disproportionation, where the formally tetravalent Bi cations disproportionate into Bi^{3+} and Bi^{5+} for the expanded and compressed octahedra, respectively [52–56]. However, Foyevtsova *et al.* recently showed, using density-functional theory calculations, that the oxygen $2p$ states are very important for the bismuthates in a very similar manner to negative charge-transfer transition-metal compounds [51]. In particular, strong hybridization between O $2p$ and Bi $6s$ states pushes antibonding states of mainly O $2p$ character with A_{1g} symmetry above the Fermi level. Under the breathing distortion, pairs of these oxygen holes then condense into A_{1g} molecular orbitals around the short bond Bi sites, in a similar nature to the E_g symmetry oxygen hole action of the nickelates.

We first show this analogy between the bismuthates and nickelates schematically in Fig. 7. For the nickelates, the E_g symmetry $d^8 \rightarrow d^7$ electron removal states are below the top of the oxygen band, and mix strongly with the E_g symmetry oxygen states near the top of the oxygen band. This leads to the distinct, antibonding E_g symmetry oxygen hole states present in the

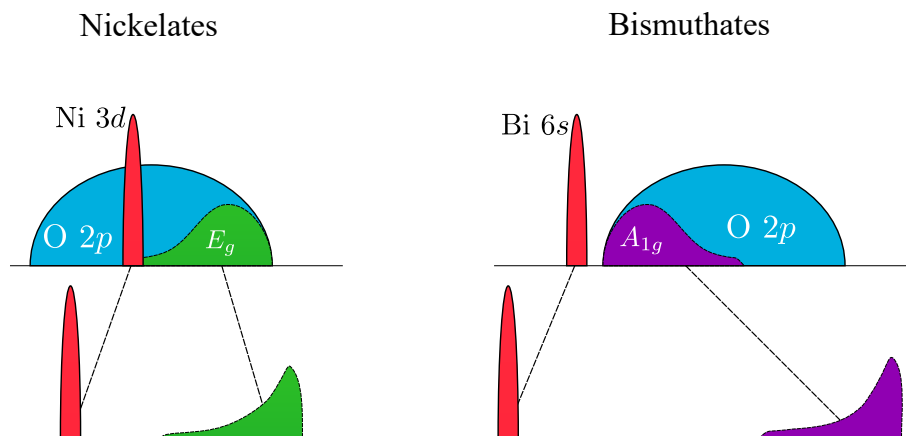


Fig. 7: Schematic showing the similarities of the perovskite nickelate and bismuthate electronic structure. In the nickelates, the Ni 3d states which have E_g symmetry mix with the oxygen 2p states of the same symmetry, which are located near the top of the valence band. Consequently, the oxygen hole states pushed out of the top of the valence band have E_g symmetry. In the bismuthates, the situation is similar, but now the relevant cation states are the Bi 6s, which are very deep. They mix strongly with the oxygen 2p states having A_{1g} symmetry which are located at the bottom of the oxygen DOS. The hybridization is very strong, leading to states of primarily oxygen 2p character and A_{1g} symmetry being pushed out of the top of the valence band. Note the cation bands are drawn with narrow widths before and after hybridization for simplicity.

nickelates, which then form molecular orbitals around short-bond Ni sites in the presence of the breathing distortion. For bismuthates the situation is very similar to the nickelates, except now the Bi 6s states are the important cation states and therefore it is states of A_{1g} rather than E_g symmetry which are important. The very deep 6s states mix very strongly with the A_{1g} oxygen 2p states, which are actually near the bottom of the oxygen band. The hybridization is strong enough, however, to push antibonding states of primarily oxygen character above the Fermi level. Again, these oxygen hole states then disproportionate under the breathing distortion, leading to the formation of A_{1g} oxygen hole molecular orbitals around the short bond Bi sites. Thus, even though the magnetic and correlation physics of the nickelates and bismuthates are drastically different, strong similarities exist regarding the importance of the oxygen 2p states in the electronic structure.

In Fig. 8, we show the actual density-functional results of Foyevtsova *et al.* [51], where the upper and lower panels contain the projected densities of states for the compressed and expanded octahedra, respectively, in the low-temperature, breathing-distorted phase of SrBiO_3 . Of particular significance is the strong, narrow conduction band of the compressed octahedron. Here the DOS projection shows that these states are of primarily O 2p character, having A_{1g} symmetry. These states are accordingly suppressed for the expanded octahedron, demonstrating the bond disproportionation that involves action of the oxygen 2p holes, rather than the typically assumed Bi charge disproportionation. It is important to note that this is a pure DFT calculation for a non-correlated material, and thus demonstrates clearly the extremely important role of the O 2p based molecular orbitals in forming the low-energy scale states, which in the end are also responsible for the superconductivity in the potassium doped materials.

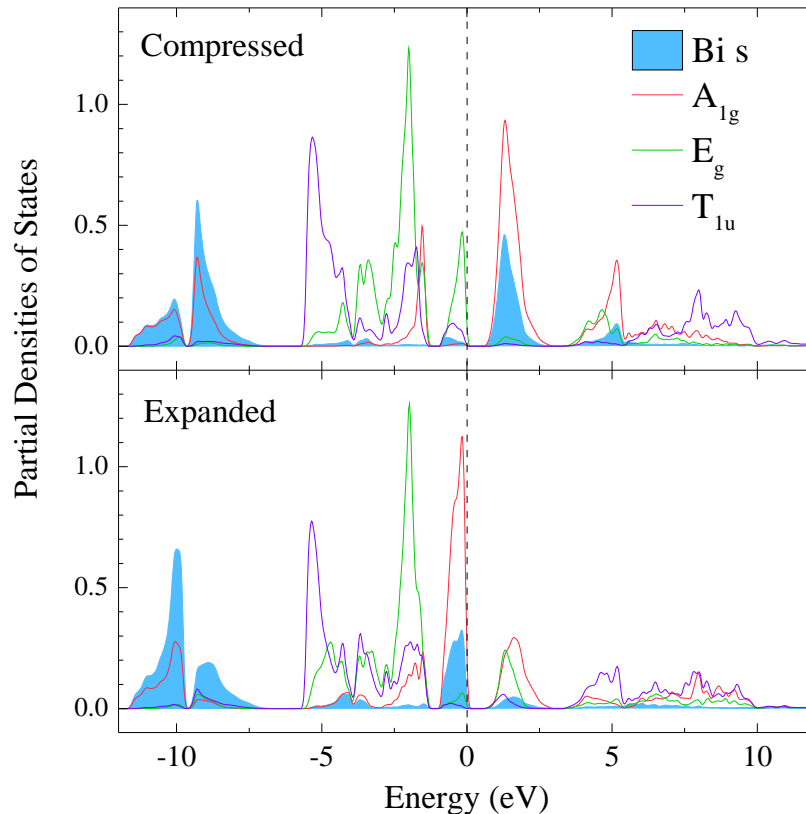


Fig. 8: Projected densities of states for the compressed (upper) and expanded (lower) octahedra in the low temperature, breathing distorted phase of SrBiO_3 .

4.3 Other negative or small charge transfer compounds

The nickelates are arguably one of the most highly studied negative charge transfer compounds at present. However, there are many other compounds which are known to be or might be negative charge transfer systems that have been studied in recent years. In fact, one of the first studies to use the term “negative charge transfer energy” was carried out by Mizokawa *et al.*, and investigated the compound NaCuO_2 [57]. As this is a sort of reference compound for the high- T_c cuprates, several groups studied the electronic structure of this material around the same time [58, 59]. Indeed, through an analysis of x-ray photoelectron spectroscopy (XPS), Mizokawa *et al.* showed that the ground state does not contain Cu^{3+} ($3d^8$) as the formal valence counting would suggest, but rather it is better described as $3d^9\bar{L}$, where again oxygen holes are present due to a negative charge transfer energy.

Other negative charge transfer compounds include the disulfide pyrites FeS_2 , CoS_2 , and NiS_2 . Here one expects that the S_2 would have a 4- valence and the cations accordingly 4+, but in fact it is found that the cations are divalent and there are accordingly missing sulfur $3p$ electrons. This leads to the formation of sulfur pairs with a net pair valence of 2- rather than 4-. In this case the antibonding S $3p$ states in the pairs are empty and therefore form rather narrow bands just above the chemical potential [60]. Accordingly, the pyrites exhibit very interesting and diverse properties: FeS_2 is a diamagnetic semiconductor, CoS_2 is a ferromagnetic metal, and

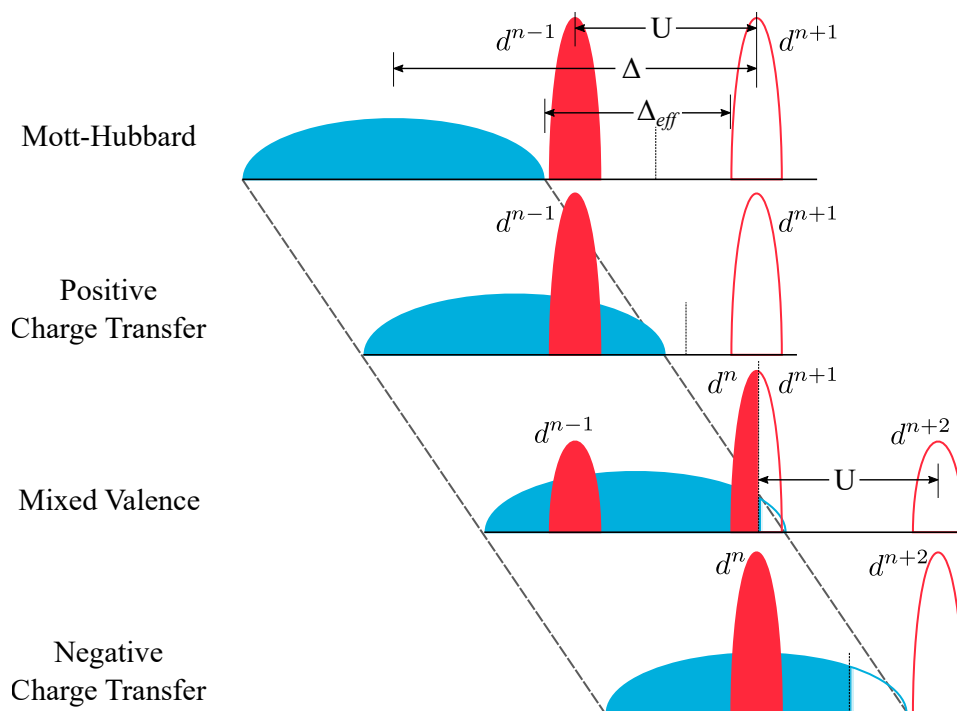


Fig. 9: The energetics of correlated compounds depicted with schematic electron removal and addition spectra in a similar nature to Fig. 4. A broad band, nominally full, is shown in blue and narrow, correlated (d) bands are shown in red. A very small hybridization is assumed between the broad and narrow bands. A constant Coulomb repulsion U separates lower and upper Hubbard bands throughout the figure. From the top to bottom, the ligand electronegativity is decreased, which can lead to different classes of compounds for the same transition-metal cations, even having the same formal valence.

NiS_2 is a Mott insulator which orders antiferromagnetically [61,62]. The electronic structures of these pyrites have been studied by various x-ray spectroscopies [60,63–66]. Further interesting properties emerge when some or all of the sulfur is substituted by Se. In particular, $\text{Ni}(\text{S}_{1-x}\text{Se}_x)_2$ is highly studied, as it exhibits a metal-insulator transition for $x = 0.23$ at $T = 0$, which changes to $x = 0.4$ at room temperature [60,67–69].

An additional highly studied negative charge transfer compound is NiS [70–72] and the related $\text{NiS}_{1-x}\text{Se}_x$ [73,74]. Here the 2+ formal valence of the Ni is not abnormally high. However, the anions S and Se have increasingly low electronegativities compared to oxygen, which also can lead to a mixed valence or a negative charge transfer energy. We show this effect schematically in Fig. 9, which is similar in nature to Fig. 4, but now we span the four classes of correlated compounds by shifting the ligand band, rather than the transition-metal bands. In this sense, moving from the positive to negative charge transfer regime in Fig. 9 would represent moving from NiO to $\text{NiS}_{1-x}\text{Se}_x$, where the formal Ni valence does not change but the ligand electronegativity does. Recent studies classify NiS as a self-doped, nearly compensated, antiferromagnetic metal [70]. It is interesting to note that researchers have been searching for Ni^{1+} oxides (although in 2D structures) in order to simulate the high- T_c cuprate electronic structure. For example, recently $\text{La}_4\text{Ni}_3\text{O}_8$ has been studied in this regard [75]. In fact, in a negative charge

transfer scenario, the Ni in NiS would be 1+ with holes in the sulfur band. In this sense it would indeed share similarities with very heavily hole-doped cuprates, having a d^9 transition-metal configuration and also a presence of ligand holes.

Moving toward the center of the $3d$ elements, the formally tetravalent Fe perovskites $A\text{FeO}_3$ with $A = \text{Ca}, \text{Sr},$ or Ba are known to have negative charge transfer energies [76–81]. This class of materials possesses a wide range of interesting properties. CaFeO_3 was found to exhibit a charge-ordered state [81], which might actually be similar to the bond-disproportionation states in the nickelates and bismuthates. $\text{SrFe}_{1-x}\text{Co}_x\text{O}_3$ is ferromagnetic and exhibits a large negative magnetoresistance [78]. $\text{La}_{1-x}\text{Sr}_x\text{FeO}_3$ with $x \approx 2/3$ also exhibits a charge disproportionation, accompanied by an order of magnitude resistivity jump and antiferromagnetic ordering [77,82]. Lastly, an example of an early $3d$ transition-metal compound with a negative charge transfer energy is CrO_2 [29]. This material has attracted significant interest as a half-metallic ferromagnet [83], and was industrially very relevant in the past as the main active component in many (now all but obsolete) magnetic recording tapes [84]. A combination of LSDA+U calculations [29] and spectroscopy [83] have verified that, even though the $3d$ electrons of the Cr have large Coulomb interactions, the material is metallic due to the negative charge transfer energy, with charge carriers at the Fermi energy having a large O $2p$ component.

5 Mixed valent rare-earth compounds

In this section, we will look at existing mixed valent compounds in detail. As mentioned earlier, the combination of correlated and band like states crossing the Fermi level in a mixed valent compound leads to a very complicated electronic structure. However, the mixed valent rare-earth compounds, such as SmB_6 and SmS have a slightly simplified description due to the very weak hybridization between the correlated $4f$ states and the broad band states. The full electronic structure is no doubt very complicated, but the weak hybridization leads to some very clear and interesting phenomena in these materials.

Samarium hexaboride was first heavily studied from the late 1960s to early 1980s. Early experimental studies of x-ray absorption [85] and susceptibility [86] measurements showed evidence that the Sm was present in both divalent and trivalent states, corresponding to f^6 and f^5 orbital occupations, respectively. Later experiments showed several interesting features, including a resistivity saturation at low temperatures and a lack of magnetic ordering down to 0.35 K [87, 88]. A similar lack of magnetism was found for SmS , which was also known to be a mixed valent compound [89]. The unique characteristics of such mixed valent compounds were analyzed with various theories, the most popular being the Anderson impurity and lattice models [90–102].

SmB_6 is now under intense study again, as recent theory work has predicted that it could be a so-called topological Kondo insulator [103, 104]. The low-temperature resistivity saturation could then be an indication of topologically protected surface states. Many experimental studies have been undertaken to test the topological insulator hypothesis (see, e.g. [105–108]), but a clear answer has yet to emerge.

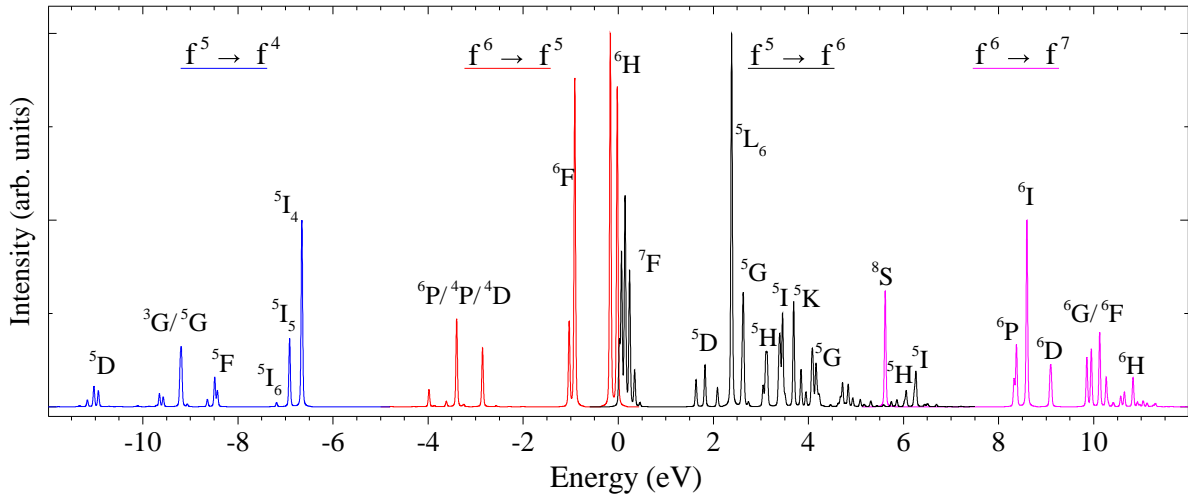


Fig. 10: Calculated f electron addition and removal spectra of mixed-valent SmB_6 . All f orbital degeneracies are included, as well as the local multiplet Coulomb interactions, which lead to the large number of excitations spread over ~ 20 eV.

The tightly contracted and highly correlated $4f$ shells of the Sm ions in SmB_6 lead to very strong multiplet effects in the electron addition and removal spectra. Further, since the complicated mixed valent ground state has components of both the f^n and f^{n+1} atomic fillings (with the lowest energy states being the Hund's rule ground states in each case), the one-electron excitation spectrum will contain four sets of features corresponding to electron addition and removal from each of the fillings (this effect was also shown schematically for the mixed-valence class in Fig. 4). In Fig. 10, we show a calculation of the multiplet rich, one-electron excitation spectrum in the atomic limit of a mixed valent Sm system. The four regions of the spectrum are indicated, and the term symbols denote the dominant contribution of each main peak (the usual $^{2S+1}L_J$ notation is used, but J is omitted in cases where different J peaks are too close to discern at this scale). There are a set of low energy excitations present near the Fermi level—since the lowest-energy f^5 and f^6 multiplets are nearly degenerate in such a mixed valent material, the one-electron removal from f^6 reaches the very low energy f^5 states, and the one-electron addition to f^5 reaches the very low energy f^6 states. However, we cannot add an electron to f^6 or remove one from f^5 at the low energy scale.

Further away from the Fermi level are the high-energy lower and upper Hubbard bands composed of $f^5 \rightarrow f^4$ and $f^6 \rightarrow f^7$ excitations, respectively. Each set of excitations is separated from the Fermi level by the Coulomb energy U , leading to a total energy separation of $2U$, as was also shown schematically in Fig. 4. An important observation from this plot are the very different intensities of the various multiplet peaks. This is of course not surprising, but the intensities of these peaks are related to the coefficients of fractional parentage (CFPs) for adding and removing electrons to/from the Hund's rule lowest energy states of the f^5 and f^6 configurations. These CFPs also play an important role in the intersite hopping of the compound, so we will investigate them in some detail in the following.

It was shown in the early work of Racah [109] that one could construct antisymmetrized eigenfunctions for a general many-electron atomic configuration l^n by using a suitable linear combination of the states obtained by angular-momentum coupling one additional electron to the eigenfunctions for the l^{n-1} configuration. The CFPs are then the coefficients of these linear combinations. One can quickly realize, then, that the required transition amplitudes between f^n and f^{n-1} configurations for calculating one-electron Green functions or hopping matrix elements will also be defined by these CFPs. An extensive tabulation of these coefficients is given by Nielson and Koster [110].

For a given f^{n-1} configuration of the correlated $4f$ shell, if we assume for now the validity of Russell-Saunders LS -coupling, we have a many-body wavefunction $|\Psi_{LSJ}^{n-1}\rangle$. The electron addition amplitude to reach a final state $|\Psi_{L'S'J'}^n\rangle$, which as stated above relates to the CFP for particular configurations, is then given by

$$\langle \Psi_{L'S'J'}^n | \mathbf{f}_{lsj}^\dagger | \Psi_{LSJ}^{n-1} \rangle \quad (4)$$

where \mathbf{f}_{lsj}^\dagger creates an f electron with the given quantum numbers. As shown for example by Hirst [111], this quantity can be written in terms of 3- j and 9- j symbols as

$$\langle \Psi_{L'S'J'}^n | \mathbf{f}_{lsj}^\dagger | \Psi_{LSJ}^{n-1} \rangle = \left[\begin{pmatrix} L & l & L' \\ -L & L-L' & L' \end{pmatrix} \begin{pmatrix} S & s & S' \\ -S & S-S' & S' \end{pmatrix} \right]^{-1} \begin{Bmatrix} L & L' & l \\ S & S' & s \\ J & J' & j \end{Bmatrix} C_{J,J',j} \quad (5)$$

where

$$C_{J,J',j} = \sqrt{(2J+1)(2J'+1)(2j+1)}. \quad (6)$$

For one-electron addition and removal spectra of a mixed valent compound, the transition rates are computed starting from the Hund's rule ground states of the f^n and f^{n-1} configurations, into all possible states that can be reached by removing or adding an electron. For the specific example of SmB_6 , as shown in Fig. 10, the starting configurations are f^5 and f^6 , and thus one can reach electron removal states of f^4 and f^5 , and electron addition states of f^6 and f^7 .

Closely related to the one-electron addition and removal spectra in a mixed valent compound are the intersite hopping integrals which couple the f^n and f^{n-1} configurations. If we define our f^n Hund's rule ground state as $|\Psi_H^n\rangle$, then it can transition to the f^{n-1} states $|\Psi_i^{n-1}\rangle$, with a total intensity of

$$I_T^- = \sum_i |\langle \Psi_i^{n-1} | \mathbf{f} | \Psi_H^n \rangle|^2 = n, \quad (7)$$

where sum rules and the degeneracy of the f shell dictate that $I_T^- = n$. In other words, the total intensity is given by the number of electrons which can be removed from the f^n configuration (for the actual hopping processes this is then scaled by the one-electron overlap integral). Similarly, the total one-electron addition intensity for the $|\Psi_H^{n-1}\rangle$ Hund's rule ground state is

$$I_T^+ = \sum_i |\langle \Psi_i^n | \mathbf{f}^\dagger | \Psi_H^{n-1} \rangle|^2 = 15 - n, \quad (8)$$

where now the sum rule depends on the number of holes available in the shell ($14 - [n - 1]$).

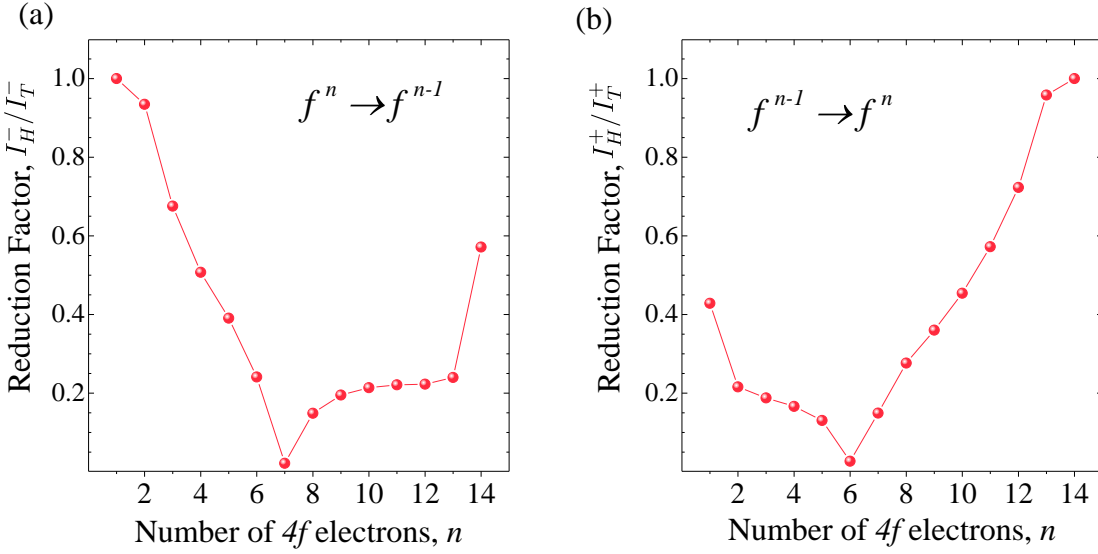


Fig. 11: Reduction factors when transition rates are restricted to Hund's rule ground states for final state. (a) Electron removal from a f^n Hund's rule ground state into a f^{n-1} Hund's rule ground state. (b) Electron addition from a f^{n-1} into a f^n state. The asymmetry between (a) and (b) arises from the degeneracy of the states.

For the mixed valent rare-earth compounds, the one-electron overlap integrals are generally very weak due to the contracted 4f radial wavefunctions. This weak hopping means that often the only important interactions to consider for the ground state are between the Hund's rule ground states of each configuration (all other higher-energy states can be neglected for the low-energy scale physics). For the case of SmB₆ these important lowest energy states are the $^6H_{5/2}$ and 7F_0 states of the f^5 and f^6 configurations, respectively. Thus the intensity integrals of Eqns. (7) and (8) can be restricted to final states corresponding to the Hund's rule ground states. We then have diminished angular matrix elements for this Hund-Hund hopping, now with a total intensity given by

$$I_H^- = \sum_{m'_j} \left| \langle \Psi_{H,m'_j}^{n-1} | \mathbf{f} | \Psi_{H,m_j}^n \rangle \right|^2 \quad (9)$$

and

$$I_H^+ = \sum_{m'_j} \left| \langle \Psi_{H,m'_j}^n | \mathbf{f}^\dagger | \Psi_{H,m_j}^{n-1} \rangle \right|^2 \quad (10)$$

where $|\Psi_{H,m_j}^n\rangle$ denotes a particular m_j Hund's rule ground state of the n electron configuration. We demonstrate the strong reduction in hopping strength that can take place in such a situation by plotting I_H^-/I_T^- and I_H^+/I_T^+ in Figs. 11(a) and 11(b), respectively. This effect was demonstrated by Hirst [111] using Eqn. (5) within the LS -coupling approximation. In Fig. 11, we show comparable results to Hirst, but now via slightly more precise exact diagonalization calculations in intermediate coupling using the code *Quanty* [45, 112–114]. From Fig. 11(a), we see there is no reduction factor for the electron removal from a f^1 configuration. This of course makes sense, since the f^0 final state is non-degenerate, so no transition intensity is lost by restricting the final state to be a Hund's rule ground state. However, one finds a very strong

reduction for both electron removal and electron addition which ends in a f^6 configuration, for example. The reason for the very strong reduction in this case is that the f^6 Hund's rule ground state is a 7F_0 singlet. This will be important for our further discussion of SmB_6 below. Finally, note that the asymmetry between the plots arises from the degeneracies of the states: a singlet 7F_0 f^6 state can hop to any of the 6 degenerate states of the ${}^6H_{5/2}$ f^5 configuration, but a particular one of those 6 only hops to the one singlet 7F_0 state. This observation is similar in nature to the “ $1/N$ ” scaling arguments used to avoid infrared divergences and solve the Anderson impurity model in earlier studies of rare-earth compounds [98–101].

As evident from Fig. 11, the hopping for such a mixed valent compound (e.g. SmB_6) can be very weak, even on top of the effect of contracted $4f$ radial wavefunctions. The importance of these angular matrix element effects is also evident from the overestimated dispersion widths in DFT calculations, which capture the contracted radial wavefunction effect, but not the CFP effect. Dispersional widths of the f bands for SmB_6 are more than an order of magnitude larger in DFT calculations compared to those found in ARPES experiments (~ 200 vs. 7 meV) [115–117].

Within the above approximations, the only f - f hopping allowed at low energy scales occurs via removing an electron from an f^6 atom and adding it to an f^5 atom, both in their Hund's rule ground states. More specifically, the f^6 atom will transition from a 7F_0 state to a ${}^6H_{5/2}$ state, and the f^5 atom will transition from a ${}^6H_{5/2}$ to a 7F_0 state. From the coefficients of fractional parentage, the transition amplitude between the 7F_0 singlet and a single m_j state of the 6-fold degenerate ${}^6H_{5/2}$ term is 0.200 times the total $f^6 \rightarrow f^5$ amplitude (where we account for the degeneracy by dividing by $\sqrt{1/6}$). Similarly, the amplitude from one of the ${}^6H_{5/2}$ states to the 7F_0 state is 0.164 times the total $f^5 \rightarrow f^6$ amplitude. Multiplying these two amplitudes for the total f - f hopping process gives a reduction factor of 0.033 for the f bandwidth compared to the one-electron bandwidth that one would obtain from DFT or LDA+U. This is in very good agreement with the discrepancy between DFT and experimental bandwidths pointed out above (200 meV vs. 7 meV, respectively).

This very strong reduction factor coming from the coefficients of fractional parentage suggests that in a first approximation we can neglect the direct f - f hopping. The d - f hopping is also reduced by the CFP effect, but only by the amplitude and not the square, so the hybridization is still important, relatively speaking. It is interesting to note that a full DMFT calculation taking into account all the multiplet structure [117] gives a bandwidth reduction of the f bands, and a reduction of the d - f hopping, consistent with the above discussion of the coefficients of fractional parentage. Note also that the phases of the coefficients of fractional parentage (which we neglected above for simplicity) could be very important. For example in manganites, similar hopping considerations which included phases found that a Berry phase is accumulated when electrons hop in loops [118].

For systems with a large U , or ones in which the splitting between the ground state and higher energy f^n configurations is large (compared to the energy scale we are considering as important), we can neglect all of the hoppings involving higher energy states when considering the lowest energy scale physics. So even the spin-orbit splitting of the f^6 manifold with $J = 0$ as the lowest energy state is large enough to neglect in zeroth order when dealing with the

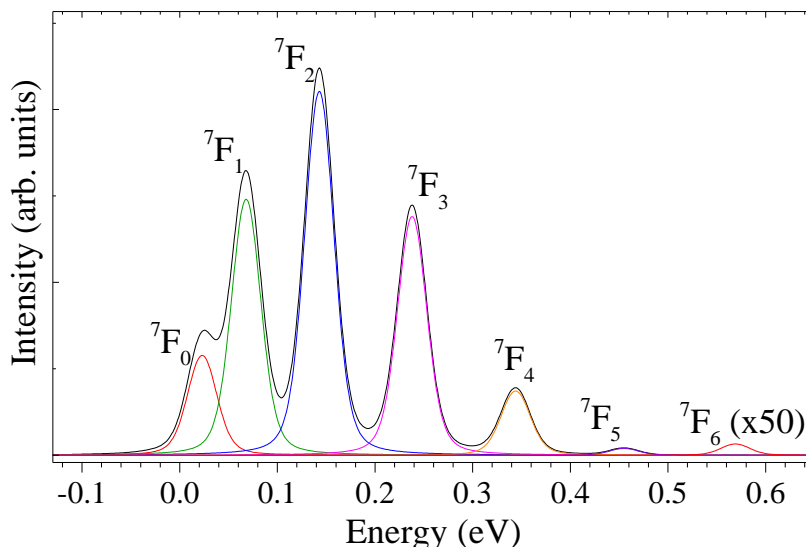


Fig. 12: The f^5 to f^6 electron addition spectrum of Fig. 10, now zoomed in to low energy scales.

low-temperature properties below 100 K. The splitting of these J states for f^6 is shown in Fig. 12, and is about 45 meV (or 520 K) for the lowest $J = 1$ excitation relative to the $J = 0$. In what follows we also neglect the crystal-field splitting within the multiplets, although this may be a bit of a stretch and a rigorous treatment should include them. Considering only the lowest-energy crystal-field states (which would likely be one of the doublets) would reduce the degeneracy to that of a Kramers doublet.

Having established the very weak hybridization present in compounds such as SmB_6 (due to both contracted radial wavefunctions and fractional-parentage matrix element effects), and that subsequently only the lowest energy f^5 and f^6 states need to be considered in a first approximation, we can now consider the band structure of the broad d band with which the f shells hybridize. Again, due to the very weak hybridization, there will only be appreciable mixing at k points near where the band crosses the f levels. We show this effect in Fig. 13, where a general light-electron band (blue) crosses the localized f level and a small hybridization is present. A small gap opens near the crossing points, and at these points the wavefunction has a true mixed character as indicated by the color of the plot. Far away from these crossing points, there is very little mixing between the f and d bands.

The schematic band structure of Fig. 13 reveals a very interesting characteristic of such materials: they are best described as mixed valent *in momentum space*. For regions of Fig. 13(a) where $|k| > 0.5\pi/a$, there are f electron removal states very close to the Fermi level. If our mixed valent compound has the valences f^{n-1} and f^n , then in these regions of momentum space the ground state is almost purely f^n . In this way, it costs very little energy to remove an electron and reach the f^{n-1} state, which is nearly degenerate with the f^n state, but we cannot add an electron within the low energy scale. As was shown in Figs. 4 and 10, to add an electron to the f^n state would cost energy U , and accordingly no such f electron addition states are present for $|k| > 0.5\pi/a$ in Fig. 13(a) (they are too high in energy to be seen).

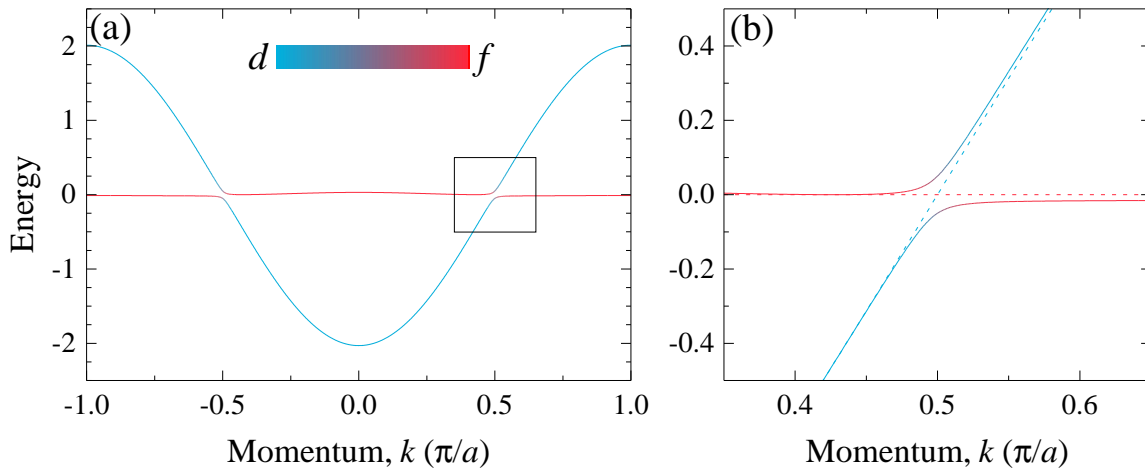


Fig. 13: Paradigmatic bandstructure of a mixed-valent rare-earth compound. A very narrow f band crosses the broad conduction band at the Fermi level. Weak hybridization opens a small gap at the band crossing points. Panel (b) shows an enlargement of the band crossing region. The color scale indicates the f and d weight in the band.

Just as the regions of momentum space where $|k| > 0.5\pi/a$ have an almost pure f^n ground state, the regions where $|k| < 0.5\pi/a$ have an almost pure f^{n-1} ground state. In this region there is an f electron addition state just above the Fermi level, as it costs essentially no energy to reach the f^n from the f^{n-1} state, but there are no f electron removal states shown as they would cost energy U and are thus far away in energy. In this sense it becomes clear that the mixed valent compound has well defined regions in momentum space with integral valences, but in fact each valence state is delocalized in real space. The many-body wave function in this situation becomes very complicated. This simple picture also indicates that a DMFT calculation which does very well in many aspects must include a strong k -dependent self energy, and in fact if a gap occurs as indicated in Figure 13, the self energy would be discontinuous or at least very strongly varying as one moves through the k region of the crossing.

In the case of SmB_6 the broad band is actually an almost equal mixture of B $2p$ states and Sm d states, as clearly shown from DFT calculations [119]. The minimum in the dispersion is at the X point in the Brillouin zone. In order to conserve charge, this band would be empty if the Sm was purely $2+$ (f^6) and would contain on average one electron per formula unit if the Sm is $3+$ (f^5). In a mixed valent situation there will be an exact compensation of f and d electrons depending on the $\text{Sm}^{2+/3+}$ ratio. If the d - f hybridization were zero then the crossing surface of the d band and the f states in momentum space would describe a Fermi surface consistent with Luttinger's theorem, as also argued by Richard Martin some time ago [120, 121]. So the surface describing the crossing point at which a gap has its largest value has the same topology as the Fermi surface one would obtain in a band theory calculation. It is an interesting question as to whether this "pseudo" Fermi surface is something that can be seen via the de Haas–van Alphen effect in high-field quantum oscillation experiments [122–125].

The above discussion provides a unique picture of the electronic structure of the low energy states of SmB_6 . This is quite different from a description in which the basic physics involves an impurity-like Kondo singlet low-energy scale state and these Kondo impurities forming a lattice which then could develop a gap and become insulating. Whether or not our above description could also be termed a “Kondo insulator” is perhaps debatable. It is also interesting to go back and have another look if perhaps other so-called heavy Fermion systems may actually fall into this category in which we rather should study things in momentum space to start with, in place of considering a lattice of Kondo impurities.

This example of the rare earths is an extreme case and can be treated in this way because of the weak hybridization. In other mixed valent systems like the actinides or the transition-metal compounds, things become very complicated because the effect of the strong hybridization between the local strongly correlated states and the broad bands crossing the Fermi energy can be very large and comparable to the band width of the broad bands. In the extreme limit of that case we would somehow be back to a DFT-based band description in which the local correlations are suppressed because of the strong hybridization with the broad bands, forming rather extended Wannier functions and diluting the effective on-site Coulomb interactions. The most interesting cases, however, are the intermediate cases which very likely involve the $3d$ transition-metal compounds such as the rare earth TM perovskite structure oxides, the ion battery materials such as LiNiO_2 , as well as the sulfides, selenides, tellurides, bromides, and iodides of the late $3d$ transition metals.

6 Summary

The central theme of this lecture is that often anion states can be much more important in correlated compounds than one would initially expect. In transition-metal compounds which have large formal oxidation states, it is often the case that the formal rules are broken. The transition metals are then better described as having more typical valences, and the anion bands are self-doped to compensate this different charge on the cations. We presented these effects through an extension of the Zaanen-Sawatzky-Allen classification scheme for transition-metal compounds. In addition to the two original classes of Mott-Hubbard and (positive) charge transfer insulators, we showed how mixed valent and negative charge transfer insulators can naturally arise. The perovskite rare-earth nickelates are a paradigmatic example of negative charge transfer compounds, where the self-doped oxygen holes make very important contributions to the conductivity and magnetism in the compounds. We also showed how similar effects can be found in non-correlated compounds such as perovskite bismuthates. Finally, we explored the interesting mixed-valence regime through the example of rare-earth compounds such as SmB_6 . Weak hybridization and mixed-valent energetics lead to the unique phenomenon of ordered valences in momentum space. A key lesson to take away from these discussions is that one might need to choose a non-conventional starting point when constructing a model to describe the electronic structure of high-valence compounds.

Acknowledgments

We thank Ilya Elfimov, Mona Berciu, Kateryna Foyevtsova, Alfred Cheung, Arash Khazraie, and Maurits Haverkort for input and helpful discussions. This article was written with the support of the Natural Sciences and Engineering Research Council of Canada, the Canadian Institute for Advanced Research, and the Max Planck–UBC Centre for Quantum Materials.

References

- [1] J.A. Yarmoff, D.R. Clarke, W. Drube, U.O. Karlsson, A. Taleb-Ibrahimi, and F.J. Himpsel, *Phys. Rev. B* **36**, 3967 (1987)
- [2] N. Nücker, J. Fink, J.C. Fuggle, P.J. Durham, and W.M. Temmerman, *Phys. Rev. B* **37**, 5158 (1988)
- [3] C.T. Chen, F. Sette, Y. Ma, M.S. Hybertsen, E.B. Stechel, W.M.C. Foulkes, M. Schuler, S.-W. Cheong, A.S. Cooper, L.W. Rupp, B. Batlogg, Y.L. Soo, Z.H. Ming, A. Krol, and Y.H. Kao, *Phys. Rev. Lett.* **66**, 104 (1991)
- [4] H. Eskes and G.A. Sawatzky, *Phys. Rev. Lett.* **61**, 1415 (1988)
- [5] F.C. Zhang and T.M. Rice, *Phys. Rev. B* **37**, 3759 (1988)
- [6] V.J. Emery and G. Reiter, *Phys. Rev. B* **38**, 4547 (1988)
- [7] B. Lau, M. Berciu, and G.A. Sawatzky, *Phys. Rev. B* **81**, 172401 (2010)
- [8] B. Lau, M. Berciu, and G.A. Sawatzky, *Phys. Rev. Lett.* **106**, 036401 (2011)
- [9] B. Lau, M. Berciu, and G.A. Sawatzky, *Phys. Rev. B* **84**, 165102 (2011)
- [10] M. Möller, G.A. Sawatzky, and M. Berciu, *Phys. Rev. B* **86**, 075128 (2012)
- [11] P. Kuiper, G. Kruizinga, J. Ghijsen, G.A. Sawatzky, and H. Verweij, *Phys. Rev. Lett.* **62**, 221 (1989)
- [12] J. van Elp, J.L. Wieland, H. Eskes, P. Kuiper, G.A. Sawatzky, F.M.F. de Groot, and T.S. Turner, *Phys. Rev. B* **44**, 6090 (1991)
- [13] J. Slater: *Quantum Theory of Atomic Structure* (McGraw-Hill, 1960)
- [14] R.D. Cowan: *The Theory of Atomic Structure and Spectra* (University of California Press, 1981)
- [15] C.J. Ballhausen: *Introduction to Ligand Field Theory* (McGraw-Hill, 1962)
- [16] I.S. Elfimov, S. Yunoki, and G.A. Sawatzky, *Phys. Rev. Lett.* **89**, 216403 (2002)
- [17] A.V. Ushakov, S.V. Streltsov, and D.I. Khomskii, *J. Phys.: Condens. Matter* **23**, 445601 (2011)
- [18] R.J. Green, M.W. Haverkort, and G.A. Sawatzky, (to be published) (2016)
- [19] J.H. de Boer and E.J.W. Verwey, *Proc. Phys. Soc.* **49**, 59 (1937)
- [20] N.F. Mott and R. Peierls, *Proc. Phys. Soc.* **49**, 72 (1937)

- [21] N.F. Mott, Proc. Phys. Soc. A **62**, 416 (1949)
- [22] J. Hubbard, Proc. R. Soc. A **277**, 237 (1964)
- [23] J. Hubbard, Proc. R. Soc. A **281**, 401 (1964)
- [24] A. Fujimori and F. Minami, Phys. Rev. B **30**, 957 (1984)
- [25] G.A. Sawatzky and J.W. Allen, Phys. Rev. Lett. **53**, 2339 (1984)
- [26] J. Zaanen, G.A. Sawatzky, and J.W. Allen, Phys. Rev. Lett. **55**, 418 (1985)
- [27] E.J.W. Verwey, Nature **144**, 327 (1939)
- [28] M.S. Senn, J.P. Wright, and J.P. Attfield, Nature **481**, 173 (2012)
- [29] M.A. Korotin, V.I. Anisimov, D.I. Khomskii, and G.A. Sawatzky, Phys. Rev. Lett. **80**, 4305 (1998)
- [30] D.I. Khomskii, Lith. J. Phys. **37**, 65 (1997)
- [31] M.L. Medarde, Journal of Physics: Condensed Matter **9**, 1679 (1997)
- [32] G. Demazeau, A. Marbeuf, M. Pouchard, and P. Hagenmuller, J. Solid State Chem. **3**, 582 (1971)
- [33] P. Lacorre, J.B. Torrance, J. Pannetier, A.I. Nazzal, P.W. Wang, and T.C. Huang, J. Solid State Chem. **91**, 225 (1991)
- [34] J.L. Garcia-Munoz, J. Rodriguez-Carvajal, P. Lacorre, and J.B. Torrance, Phys. Rev. B **46**, 4414 (1992)
- [35] J.B. Torrance, P. Lacorre, A.I. Nazzal, E.J. Ansaldo, and C. Niedermayer, Phys. Rev. B **45**, 8209 (1992)
- [36] A. Frano, E. Schierle, M.W. Haverkort, Y. Lu, M. Wu, S. Blanco-Canosa, U. Nwankwo, A.V. Boris, P. Wochner, G. Cristiani, H.U. Habermeier, G. Logvenov, V. Hinkov, E. Benckiser, E. Weschke, and B. Keimer, Phys. Rev. Lett. **111**, 106804 (2013)
- [37] A.V. Boris, Y. Matiks, E. Benckiser, A. Frano, P. Popovich, V. Hinkov, P. Wochner, M. Castro-Colin, E. Detemple, V.K. Malik, C. Bernhard, T. Prokscha, A. Suter, Z. Salman, E. Morenzoni, G. Cristiani, H.U. Habermeier, and B. Keimer, Science **332**, 937 (2011)
- [38] E. Benckiser, M.W. Haverkort, S. Brueck, E. Goering, S. Macke, A. Frano, X. Yang, O.K. Andersen, G. Cristiani, H.-U. Habermeier, A.V. Boris, I. Zegkinoglou, P. Wochner, H.-J. Kim, V. Hinkov, and B. Keimer, Nat. Mater. **10**, 189 (2011)

- [39] J. Liu, M. Kargarian, M. Kareev, B. Gray, P.J. Ryan, A. Cruz, N. Tahir, Y.-D. Chuang, J. Guo, J.M. Rondinelli, J.W. Freeland, G.A. Fiete, and J. Chakhalian, *Nat. Commun.* **4**, 2714 (2013)
- [40] S. Catalano, M. Gibert, V. Bisogni, O.E. Peil, F. He, R. Sutarto, M. Viret, P. Zubko, R. Scherwitzl, A. Georges, G.A. Sawatzky, T. Schmitt, and J.-M. Triscone, *APL Mater.* **2**, 116110 (2014)
- [41] T. Mizokawa, D.I. Khomskii, and G.A. Sawatzky, *Phys. Rev. B* **61**, 11263 (2000)
- [42] H. Park, A.J. Millis, and C.A. Marianetti, *Phys. Rev. Lett.* **109**, 156402 (2012)
- [43] S. Johnston, A. Mukherjee, I. Elfimov, M. Berciu, and G.A. Sawatzky, *Phys. Rev. Lett.* **112**, 106404 (2014)
- [44] F.M.F. de Groot and A. Kotani: *Core Level Spectroscopy of Solids* (CRC Press, Taylor & Francis Group, 2008)
- [45] M.W. Haverkort, M. Zwierzycki, and O.K. Andersen, *Phys. Rev. B* **85**, 165113 (2012)
- [46] J. Zaanen, C. Westra, and G.A. Sawatzky, *Phys. Rev. B* **33**, 8060 (1986)
- [47] M. Medarde, A. Fontaine, J.L. García-Muñoz, J. Rodríguez-Carvajal, M. de Santis, M. Sacchi, G. Rossi, and P. Lacorre, *Phys. Rev. B* **46**, 14975 (1992)
- [48] C. Piamonteze, F.M.F. de Groot, H.C.N. Tolentino, A.Y. Ramos, N.E. Massa, J.A. Alonso, and M.J. Martínez-Lope, *Phys. Rev. B* **71**, 020406 (2005)
- [49] J.W. Freeland, M. van Veenendaal, and J. Chakhalian, *Journal of Electron Spectroscopy and Related Phenomena* **208**, 56 (2015)
- [50] T. Mizokawa, A. Fujimori, T. Arima, Y. Tokura, N. Mōri, and J. Akimitsu, *Phys. Rev. B* **52**, 13865 (1995)
- [51] K. Foyevtsova, A. Khazraie, I. Elfimov, and G.A. Sawatzky, *Phys. Rev. B* **91**, 121114 (2015)
- [52] T.M. Rice and L. Sneddon, *Phys. Rev. Lett.* **47**, 689 (1981)
- [53] D. Cox and A. Sleight, *Solid State Commun.* **19**, 969 (1976)
- [54] D.E. Cox and A.W. Sleight, *Acta Crystallographica B* **35**, 1 (1979)
- [55] C.M. Varma, *Phys. Rev. Lett.* **61**, 2713 (1988)
- [56] I. Hase and T. Yanagisawa, *Phys. Rev. B* **76**, 174103 (2007)
- [57] T. Mizokawa, H. Namatame, A. Fujimori, K. Akeyama, H. Kondoh, H. Kuroda, and N. Kosugi, *Phys. Rev. Lett.* **67**, 1638 (1991)

- [58] D.D. Sarma, O. Strebler, C.T. Simmons, U. Neukirch, G. Kaindl, R. Hoppe, and H.P. Müller, *Phys. Rev. B* **37**, 9784 (1988)
- [59] K. Karlsson, O. Gunnarsson, and O. Jepsen, *J. Phys.: Condens. Matter* **4**, 2801 (1992)
- [60] W. Folkerts, G.A. Sawatzky, C. Haas, R.A. de Groot, and F.U. Hillebrecht, *J. Phys. C: Solid State Physics* **20**, 4135 (1987)
- [61] K. Adachi, K. Sato, and M. Takeda, *J. Phys. Soc. Japan* **26**, 631 (1969)
- [62] S. Ogawa, *J. Appl. Phys.* **50**, 2308 (1979)
- [63] A.E. Bocquet, K. Mamiya, T. Mizokawa, A. Fujimori, T. Miyadai, H. Takahashi, M. Mōri, and S. Suga, *J. Phys.: Condens. Matter* **8**, 2389 (1996)
- [64] A. Fujimori, K. Mamiya, T. Mizokawa, T. Miyadai, T. Sekiguchi, H. Takahashi, N. Mōri, and S. Suga, *Phys. Rev. B* **54**, 16329 (1996)
- [65] J. Kanamori, A. Okiji, H. Shiba, K. Terakura, K. Mamiya, T. Mizokawa, A. Fujimori, H. Takahashi, N. Mori, T. Miyadai, S. Suga, N. Chandrasekharan, S. Krishnakumar, and D. Sarma, *Physica B* **237**, 390 (1997)
- [66] K. Mamiya, T. Mizokawa, A. Fujimori, T. Miyadai, N. Chandrasekharan, S.R. Krishnakumar, D.D. Sarma, H. Takahashi, N. Mōri, and S. Suga, *Phys. Rev. B* **58**, 9611 (1998)
- [67] J. Mazzaferro, H. Ceva, and B. Alascio, *Phys. Rev. B* **22**, 353 (1980)
- [68] J.A. Wilson: *The Metallic and Non-Metallic States of Matter* (London: Taylor and Francis, 1985) p. 215
- [69] A. Ferraz, R. Chapman, N. March, B. Alascio, and C. Sayers, *Solid State Commun.* **57**, 937 (1986)
- [70] S.K. Panda, I. Dasgupta, E. Sasioglu, S. Blügel, and D.D. Sarma, *Sci. Rep.* (2013)
- [71] S.K. Panda, P. Thunström, I.D. Marco, J. Schött, A. Delin, I. Dasgupta, O. Eriksson, and D.D. Sarma, *New J. Phys.* **16**, 093049 (2014)
- [72] M. Nakamura, A. Fujimori, M. Sacchi, J.C. Fuggle, A. Misu, T. Mamori, H. Tamura, M. Matoba, and S. Anzai, *Phys. Rev. B* **48**, 16942 (1993)
- [73] D.D. Sarma, S.R. Krishnakumar, N. Chandrasekharan, E. Weschke, C. Schüßler-Langeheine, L. Kilian, and G. Kaindl, *Phys. Rev. Lett.* **80**, 1284 (1998)
- [74] S.R. Krishnakumar, N. Shanthi, P. Mahadevan, and D.D. Sarma, *Phys. Rev. B* **61**, 16370 (2000)

- [75] V.V. Poltavets, K.A. Lokshin, A.H. Nevidomskyy, M. Croft, T.A. Tyson, J. Hadermann, G. Van Tendeloo, T. Egami, G. Kotliar, N. ApRoberts-Warren, A.P. Dioguardi, N.J. Curro, and M. Greenblatt, *Phys. Rev. Lett.* **104**, 206403 (2010)
- [76] A.E. Bocquet, A. Fujimori, T. Mizokawa, T. Saitoh, H. Namatame, S. Suga, N. Kimizuka, Y. Takeda, and M. Takano, *Phys. Rev. B* **45**, 1561 (1992)
- [77] A. Chainani, M. Mathew, and D.D. Sarma, *Phys. Rev. B* **48**, 14818 (1993)
- [78] M. Abbate, G. Zampieri, J. Okamoto, A. Fujimori, S. Kawasaki, and M. Takano, *Phys. Rev. B* **65**, 165120 (2002)
- [79] N. Hayashi, T. Yamamoto, H. Kageyama, M. Nishi, Y. Watanabe, T. Kawakami, Y. Matsushita, A. Fujimori, and M. Takano, *Angewandte Chemie* **123**, 12755 (2011)
- [80] T. Tsuyama, T. Matsuda, S. Chakraverty, J. Okamoto, E. Ikenaga, A. Tanaka, T. Mizokawa, H.Y. Hwang, Y. Tokura, and H. Wadati, *Phys. Rev. B* **91**, 115101 (2015)
- [81] T. Akao, Y. Azuma, M. Usuda, Y. Nishihata, J. Mizuki, N. Hamada, N. Hayashi, T. Terashima, and M. Takano, *Phys. Rev. Lett.* **91**, 156405 (2003)
- [82] H. Wadati, A. Chikamatsu, R. Hashimoto, M. Takizawa, H. Kumigashira, A. Fujimori, M. Oshima, M. Lippmaa, M. Kawasaki, and H. Koinuma, *J. Phys. Soc. Jpn* **75**, 054704 (2006)
- [83] D.J. Huang, L.H. Tjeng, J. Chen, C.F. Chang, W.P. Wu, S.C. Chung, A. Tanaka, G.Y. Guo, H.-J. Lin, S.G. Shyu, C.C. Wu, and C.T. Chen, *Phys. Rev. B* **67**, 214419 (2003)
- [84] G. Bate, *IEEE Transactions on Magnetics* **14**, 136 (1978)
- [85] E.E. Vainshtein, S.M. Vlokhin, and Y.B. Paderno, *Fiz. Tverd. Tela* **6**, 2909 (1964)
- [86] Y.B. Paderno, S. Pokrzywnicki, and B. Stalinski, *Phys. Status Solidi* **24**, K73 (1967)
- [87] A. Menth, E. Buehler, and T.H. Geballe, *Phys. Rev. Lett.* **22**, 295 (1969)
- [88] J.W. Allen, B. Batlogg, and P. Wachter, *Phys. Rev. B* **20**, 4807 (1979)
- [89] M.B. Maple and D. Wohlleben, *Phys. Rev. Lett.* **27**, 511 (1971)
- [90] L.L. Hirst, *Physik der kondensierten Materie* **11**, 255 (1970)
- [91] C.M. Varma and Y. Yafet, *Phys. Rev. B* **13**, 2950 (1976)
- [92] D. Khomskii and A. Kocharjan, *Solid State Commun.* **18**, 985 (1976)
- [93] A.N. Kockaryan and D.I. Khomskii, *JETP* **44**, 404 (1976)
- [94] C.M. Varma, *Rev. Mod. Phys.* **48**, 219 (1976)

- [95] L.L. Hirst, Phys. Rev. B **15**, 1 (1977)
- [96] F.D.M. Haldane, Phys. Rev. B **15**, 2477 (1977)
- [97] R.M. Martin and J.W. Allen, J. Appl. Phys. **50**, 7561 (1979)
- [98] H.R. Krishna-murthy, J.W. Wilkins, and K.G. Wilson, Phys. Rev. B **21**, 1003 (1980)
- [99] H.R. Krishna-murthy, J.W. Wilkins, and K.G. Wilson, Phys. Rev. B **21**, 1044 (1980)
- [100] O. Gunnarsson and K. Schönhammer, Phys. Rev. B **28**, 4315 (1983)
- [101] O. Gunnarsson and K. Schönhammer, Phys. Rev. Lett. **50**, 604 (1983)
- [102] P. Coleman, Phys. Rev. B **29**, 3035 (1984)
- [103] M. Dzero, K. Sun, V. Galitski, and P. Coleman, Phys. Rev. Lett. **104**, 106408 (2010)
- [104] V. Alexandrov, M. Dzero, and P. Coleman, Phys. Rev. Lett. **111**, 226403 (2013)
- [105] D.J. Kim, S. Thomas, T. Grant, J. Botimer, Z. Fisk, and J. Xia, Scientific Reports **3**, 3150 (2013)
- [106] S. Wolgast, C. Kurdak, K. Sun, J.W. Allen, D.-J. Kim, and Z. Fisk, Phys. Rev. B **88**, 180405 (2013)
- [107] X. Zhang, N.P. Butch, P. Syers, S. Ziemak, R.L. Greene, and J. Paglione, Phys. Rev. X **3**, 011011 (2013)
- [108] Z.-H. Zhu, A. Nicolaou, G. Levy, N.P. Butch, P. Syers, X.F. Wang, J. Paglione, G.A. Sawatzky, I.S. Elfimov, and A. Damascelli, Phys. Rev. Lett. **111**, 216402 (2013)
- [109] G. Racah, Phys. Rev. **63**, 367 (1943)
- [110] C.W. Nielson and G.F. Koster: *Spectroscopic coefficients for the p^n , d^n , and f^n configurations* (MIT Press, 1963)
- [111] L.L. Hirst, Phys. Rev. B **15**, 1 (1977)
- [112] M.W. Haverkort et al.: <http://www.quanty.org>
- [113] Y. Lu, M. Höppner, O. Gunnarsson, and M.W. Haverkort, Phys. Rev. B **90**, 085102 (2014)
- [114] M.W. Haverkort, G. Sangiovanni, P. Hansmann, A. Toschi, Y. Lu, and S. Macke, Europhys. Lett. **108**, 57004 (2014)
- [115] J. Kim, K. Kim, C.-J. Kang, S. Kim, H.C. Choi, J.-S. Kang, J.D. Denlinger, and B.I. Min, Phys. Rev. B **90**, 075131 (2014)

- [116] J.D. Denlinger, J.W. Allen, J.-S. Kang, K. Sun, B.I. Min, D.J. Kim, and Z. Fisk, *JPS Conf. Proc.* **3**, 017038 (2014)
- [117] J.D. Denlinger, J.W. Allen, J.-S. Kang, K. Sun, J.-W. Kim, J.H. Shim, B.I. Min, D.-J. Kim, and Z. Fisk, arXiv:1312.6637
- [118] E. Müller-Hartmann and E. Dagotto, *Phys. Rev. B* **54**, R6819 (1996)
- [119] I. Elfimov, Private Communication
- [120] R.M. Martin, *Phys. Rev. Lett.* **48**, 362 (1982)
- [121] R.M. Martin, *Journal of Applied Physics* **53**, 2134 (1982)
- [122] B.S. Tan, Y.-T. Hsu, B. Zeng, M.C. Hatnean, N. Harrison, Z. Zhu, M. Hartstein, M. Kiourlappou, A. Srivastava, M.D. Johannes, T.P. Murphy, J.-H. Park, L. Balicas, G.G. Lonzarich, G. Balakrishnan, and S.E. Sebastian, *Science* **349**, 287 (2015)
- [123] J. Knolle and N.R. Cooper, *Phys. Rev. Lett.* **115**, 146401 (2015)
- [124] O. Erten, P. Ghaemi, and P. Coleman, *Phys. Rev. Lett.* **116**, 046403 (2016)
- [125] L. Zhang, X.-Y. Song, and F. Wang, *Phys. Rev. Lett.* **116**, 046404 (2016)

